The Journal of Neuroscience, November 1990, 10(11): 3664–3684

Colocalization of Ion Channels Involved in Frequency Selectivity and Synaptic Transmission at Presynaptic Active Zones of Hair Cells

William M. Roberts,[1] R. A. Jacobs,[2] and A. J. Hudspeth[2]

[1]Institute of Neuroscience, University of Oregon, Eugene, Oregon 97403 and [2]Department of Cell Biology and Neuroscience, University of Texas Southwestern Medical Center, Dallas, Texas 75235-9039

Calcium ions serve as intracellular messengers in 2 activities of hair cells: in conjunction with Ca^{2+}-activated K^+ channels, they produce the electrical resonance that tunes each cell to a specific frequency of stimulation, and they trigger the release of a chemical synaptic transmitter. Our experiments indicate that both of these functions are conducted within a region that extends a few hundred nanometers around each presynaptic active zone. In focal electrical recordings from the plasma membranes of isolated anuran hair cells, we found nearly all of a cell's Ca^{2+} channels and Ca^{2+}-activated K^+ channels clumped at a fixed ratio in an average of 20 clusters on the basolateral membrane surface. Because serial-section electron microscopy indicated that each hair cell has ~19 afferent synaptic contacts with a similar distribution upon its basolateral surface, we conclude that the channel clusters coincide with synaptic active zones. Ensemble-variance analysis of current fluctuations indicated that each cell has a total of ~1800 Ca^{2+} channels and ~700 Ca^{2+}-activated K^+ channels; if these are uniformly divided, we estimate that each channel cluster contains ~90 Ca^{2+} and ~40 Ca^{2+}-activated K^+ channels. Freeze-fracture electron microscopy demonstrated an average of 133 large intramembrane particles in the presynaptic membrane at each active zone, an observation that suggests that the particles are the clustered channels. We used the K^+ channel's sensitivity to intracellular Ca^{2+} to assay the concentration of free Ca^{2+} in the presynaptic cytoplasm, which we found to vary between 10 μM and 1 mM over the physiological range of membrane potentials. The inferred concentrations agreed with the values predicted for free diffusion of Ca^{2+} away from Ca^{2+} channels scattered randomly within a 300-nm-diameter synaptic active zone. The close association among Ca^{2+} channels, Ca^{2+}-activated K^+ channels, and synaptic active zones is necessary both for the rapid activation of K^+ currents required in electrical resonance and for the transmission at afferent synapses of information about the phases of high-frequency stimuli.

Received May 22, 1990; revised July 24, 1990; accepted July 27, 1990.

The authors thank Drs. J. L. Allen, P. G. Gillespie, J. Howard, and L. F. A. Jaramillo, Ms. S. K. H. Gillespie, and Mr. D. M. Raizen for comments on the manuscript. The initial experiments were performed in the Department of Physiology at the University of California, San Francisco. The study was supported by NIH Grants NS22389 and DC00317, the System Development Foundation, and the Perot Family Foundation.

Correspondence should be addressed to Dr. A. J. Hudspeth, Department of Cell Biology and Neuroscience, Box 9039, University of Texas Southwestern Medical Center, 5323 Harry Hines Boulevard, Dallas, TX 75235-9039.

Stimulation of the auditory, vestibular, and lateral-line sensory organs of vertebrates excites mechanoreceptive hair cells, which encode the amplitude, frequency, and direction of mechanical stimuli. Like many other sensory receptors, each hair cell performs 3 basic physiological functions: it transduces a stimulus into an intracellular electrical signal, it filters the stimulus or the response to enhance frequencies of behavioral importance, and it synaptically transmits information to the CNS. Each of these functions is mediated by specific types of ion channels in the hair cell's plasma membrane (for reviews, see Hudspeth, 1986, 1989; Howard et al., 1988; Roberts et al., 1988). In this paper, we describe the topographical locations of these channels on the cellular surface and consider the implications of these distributions for transduction, tuning, and transmission.

Mechanoelectrical transduction commences when a stimulus parallel to the hair cell's apical surface deflects the hair bundle, a staircase array of force-sensitive stereocilia. The hair bundle is sensitive only to the stimulus component parallel to a line between the bundle's shortest and tallest edges. Deflection in the positive direction, towards the bundle's tall edge, augments the inward receptor current by opening mechanoelectrical transduction channels in the hair bundle; deflection in the opposite direction closes the channels that were open in the unstimulated cell. Directional sensitivity probably results from the orientation within the hair bundle of gating springs, elastic linkages that transmit forces to the channels' gates and are stretched by deflections in the positive direction (for reviews, see Howard et al., 1988; Roberts et al., 1988; Hudspeth, 1989). One result of the present study, that stereocilia are efficient cables for the transmission of electrical signals, is consistent with other evidence that mechanoelectrical transduction occurs near the hair bundle's tip (Hudspeth, 1982).

To enhance their responsiveness to stimuli of appropriate frequencies, the hair cells in many organs act as electrical resonators that respond best to stimulation within a narrow band of frequencies (Crawford and Fettiplace, 1981; Lewis and Hudspeth, 1983a; Fuchs et al., 1988; Sugihara and Furukawa, 1989; for a review, see Fettiplace, 1987). Resonance results from the interplay of 2 types of ion channels: Ca^{2+} channels that are opened by depolarization, and Ca^{2+}-activated K^+ channels that are opened cooperatively by depolarization and Ca^{2+} that enters a cell through the Ca^{2+} channels (Lewis and Hudspeth, 1983a,b; Ashmore and Attwell, 1985; Art and Fettiplace, 1987; Hudspeth and Lewis, 1988a,b). Because electrical tuning operates at frequencies up to at least 440 Hz (Crawford and Fettiplace, 1981), the time required for Ca^{2+} ions to diffuse from the mouth of a Ca^{2+} channel to binding sites on Ca^{2+}-activated K^+ channels is of crucial importance (Hudspeth and Lewis, 1988b). In the study

Table 1. Internal solutions for physiological recording

Solution	K^+ (mM)	Cs^+ (mM)	Ca^{2+} (μM)	Mg^{2+} (mM)	Aspartate (mM)	Cl^- (mM)	HEPES (mM)	ATP (mM)	Buffer (mM)	Free Ca^{2+} (M)	Free K^+ (mM)	Osmotic strength (mmol kg^{-1})	V_{jp} (mV)
K^+-aspartate (EGTA)	116	—	78	2.0	106	4.2	5	1	1	$\sim10^{-8}$	104	210	−13
Cs^+-aspartate (EGTA)	—	116	78	2.0	106	4.2	5	1	1	$\sim10^{-8}$	—	210	−3
Ca^{2+}-free (BAPTA)	~264	—	—	8.0	—	16.0	5	1	~66	$<10^{-9}$	—	205	−13
Ca^{2+}-free (Br_2BAPTA)	~160	—	—	2.2	—	4.4	10	1	~40	$<10^{-9}$	78	224	−14
High-Ca^{2+} (Br_2BAPTA)	~160	—	~40	2.0	—	4.0	10	1	~40	10^{-4}	78	214	−12

In solutions containing BAPTA or Br_2BAPTA as the Ca^{2+} buffer, the total concentration of K_4-BAPTA or K_4-Br_2BAPTA in solution was not determined precisely because of the procedure used to adjust osmotic strength. Free Ca^{2+} and K^+ concentrations were measured using ion-selective electrodes calibrated against standards (Oriel Research Inc., Boston, MA) diluted with double-distilled water. The total Mg^{2+} concentration in each internal solution was calculated from equilibrium dissociation constants (Martell and Smith, 1974; Tsien, 1980) to yield a free Mg^{2+} concentration of 2 mM; the free Mg^{2+} concentration was not measured. The pH of each internal solution was adjusted to 7.20–7.25. Osmotic strength was measured using a vapor-pressure osmometer. Junctional potentials were measured relative to the extracellular saline solution using a 3-M KCl reference electrode.

reported here, we mapped the locations of ion channels on the cellular surface in order to ascertain whether their distribution is optimal for electrical resonance.

The hair cell's third function, synaptic transmission, remains poorly understood. Electron microscopic studies indicate that individual hair cells in various species contain from 1 to nearly 100 presynaptic active zones (Miller and Beck, 1988), each associated with a swarm of synaptic vesicles and at least 1 synaptic body, a spherical, osmiophilic structure of unknown function that resembles the presynaptic specializations of photoreceptors and certain neurons. Synaptic transmission occurs by quantal release (Ishii et al., 1971) of an unknown neurotransmitter, probably an amino acid (Cochran et al., 1987; but see Sewell and Mroz, 1987; for reviews, see Bledsoe, 1986; Roberts et al., 1988). As at other chemical synapses, the entry of Ca^{2+} through voltage-gated channels presumably initiates the release of transmitter. The mapping experiments presented in this paper suggest that most, and possibly all, of the clusters of Ca^{2+} channels and Ca^{2+}-activated K^+ channels coincide with presynaptic active zones; the Ca^{2+} channels in these clusters evidently participate in both electrical tuning and transmitter release.

Materials and Methods

We studied electrically resonant hair cells from the sacculi of grass frogs, *Rana pipiens*. Such cells sense low-frequency, groundborne vibrations *in vivo* (Koyama et al., 1982) and continue to exhibit sharp electrical tuning after dissociation *in vitro* (Lewis and Hudspeth, 1983a).

The general experimental procedures have been described in detail (Kroese et al., 1989). Hair cells dissociated enzymatically with papain (Lewis and Hudspeth, 1983a; Hudspeth and Lewis, 1988a) were allowed to settle onto the coverglass bottom of a 500-μl experimental chamber. The cells were observed with a mechanically stabilized, inverted microscope (IM35, Carl Zeiss, Oberkochen, FRG) equipped with a 63× oil-immersion objective lens (numerical aperture 1.4), a 40× water-immersion objective lens for the condenser (numerical aperture 0.75), and differential-interference-contrast optics. The chamber was perfused continuously with standard extracellular saline solution containing 110 mM Na^+, 2 mM K^+, 4 mM Ca^{2+}, 118 mM Cl^-, 5 mM HEPES, and 3 mM D-glucose. The pH was adjusted to 7.25; the osmotic strength was 220 mmol kg^{-1}. Pharmacological agents were added to the perfusate without ionic substitution. All experiments were carried out at room temperature (22–25°C). A PDP-11/73 computer (Digital Equipment Corp., Maynard, MA) with a Laboratory Display System and BASIC-23 programming language (INDEC Systems, Sunnyvale, CA) was used to generate voltage-clamp commands, record currents, analyze data, and display results.

Whole-cell voltage-clamp recording. Recordings of whole-cell current were made with a voltage-clamp amplifier (EPC-7, List-Electronic, Darmstadt, FRG) through glass pipettes tightly sealed to the cell surface (Sakmann and Neher, 1983). Pipettes were pulled from capillary tubing (R-6 soda-lime glass, Garner Glass Co., Claremont, CA), coated with silicone plastic (Sylgard 182, Dow Chemical Co., Midland, MI) to reduce capacitance, heat polished to tip diameters of 1–2 μm immediately before use, and filled with internal solution. After a seal with a leakage resistance in excess of 1 GΩ was formed, the subjacent membrane patch was ruptured by a suction transient; the series access resistance was thereafter generally less than 10 MΩ. Sealing was occasionally improved by sucking into the pipette's tip about 1 μl of internal solution containing 1 mM gentamicin sulfate. Although this solution was expelled by pressure before sealing, some of the drug evidently adsorbed to the pipette wall, where it promoted sealing by an unknown mechanism (Holton and Hudspeth, 1986).

The components of the internal solutions are shown in Table 1. Free Ca^{2+} concentrations of 1 μM and 10 μM were achieved by mixing stock solutions that contained free Ca^{2+} concentrations of 0 μM and 100 μM, buffered with 40 mM 5,5′-dibromo-1,2-bis(*o*-aminophenoxy)ethane-*N,N,N′,N′*-tetraacetic acid (Br_2BAPTA, Molecular Probes, Eugene, OR). Br_2BAPTA was used because its K_d for Ca^{2+} is 1–5 μM, close to the desired free Ca^{2+} concentration, and its affinities for Mg^{2+} and H^+ are much lower than that for Ca^{2+} (Tsien, 1980). Essentially Ca^{2+}-free internal solution was buffered with 66 mM 1,2-bis(*o*-aminophenoxy)ethane-*N,N,N′,N′*-tetraacetic acid (BAPTA, Molecular Probes). The internal solution containing 1 mM free Ca^{2+} was made by adding $CaCl_2$ to the standard K^+-aspartate internal solution. Because most of the internal solutions used in whole-cell recordings contained large anions that diffused more slowly than the accompanying cations, we measured and corrected for the liquid junction potentials (V_{jp}) at the pipettes' tips (Marty and Neher, 1983). Values of V_{jp} are given in Table 1. Had we neglected to correct for the junction potentials, membrane potentials would have appeared 12–14 mV more positive in all but the Cs^+-aspartate internal saline.

Focal current recordings to map channel distributions. In some whole-cell voltage-clamp experiments, we used a second, 1–10-μm-diameter, cell-attached pipette to record focal membrane currents during whole-cell stimulation (Roberts and Hudspeth, 1987a,b; Roberts et al., 1990). The focal pipette was pulled from the same type of glass as the whole-cell pipette, coated and polished as above, and filled with the bath saline solution. This electrode was connected to a voltage-clamp amplifier used as a virtual-ground current monitor that measured the patch current through a 10-MΩ resistor (Roberts, 1987). By applying ~1-mV voltage steps to the focal pipette, we measured the pipette resistance before, and the seal resistance after, making contact with the cell surface. To allow for the resistance of the solution outside the pipette, the series-resistance compensation was set ~10% below the pipette's measured resistance (Roberts, 1987).

We purposefully avoided using tightly sealed focal pipettes because they distorted the cellular surface, often pulling a bleb of membrane and cytoplasm containing particles in Brownian motion several micrometers into the pipette (Fig. 1*A*; Sakmann and Neher, 1983). Because we were concerned that blebbing might perturb the local current density by increasing membrane area, releasing ion channels from cytoskeletal anchorages (Tank et al., 1982), or altering Ca^{2+} buffering and extrusion, we treated the focal pipettes to prevent formation of tight seals. Some

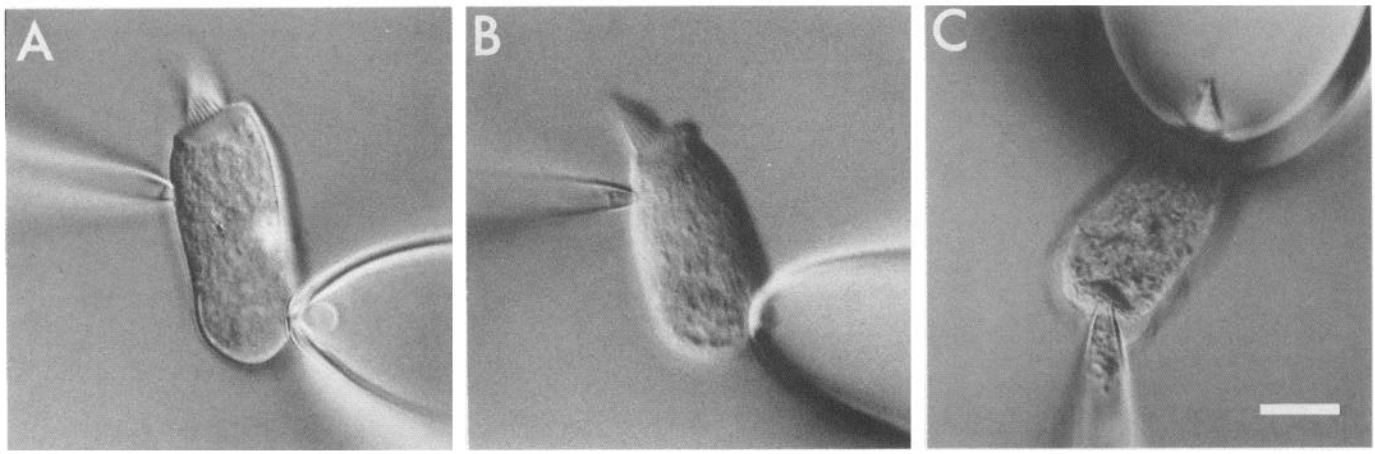

Figure 1. Experimental preparations used to record focal membrane currents from voltage-clamped hair cells. In each instance, a tightly sealed, whole-cell pipette (*left* in *A* and *B*, *bottom* in *C*) applied voltage steps and recorded the whole-cell current, while a loosely sealed pipette measured the focal current. *A*, The gentle suction (~1 kPa) needed to maintain a stable seal pulled a bleb of membrane into a conventional patch pipette. *B*, No bleb was formed in a loosely sealed pipette with a collagen plug precipitated at its tip. *C*, During recordings of the current through the apical membrane, including the stereociliary membrane, a large, loosely sealed pipette engulfed the hair cell's entire apical surface. Scale bar, 10 μm for *A–C*.

pipettes were dipped into a saline solution to which 1 gm·l^{-1} bovine serum albumin had been added. Others were plugged with collagen by sucking a few microliters of a solution of 1 gm·l^{-1} rat-tail collagen dissolved in 18 mM acetic acid into each pipette tip and allowing the solvent to evaporate. The network of collagen fibers prevented blebbing (Fig. 1*B*) without noticeably increasing the pipette's electrical resistance. Such a pipette formed a loose seal (Stühmer et al., 1983), usually with a resistance of 1–5 MΩ, that provided only partial electrical isolation of the underlying membrane patch. Careful compensation for the resistances of the focal pipette and the silver-silver chloride junctions in the pipette holder and bath ground eliminated most of the errors associated with the loose seal (Roberts, 1987). The remaining source of error, the extracellular field potential, is discussed below.

This approach could be extended to record from a large portion of a cell's surface, such as the entire apical membrane (Fig. 1*C*). A similar technique has been employed to isolate the apical-membrane currents of gustatory receptors (Kinnamon et al., 1988).

Extracellular field potentials. During voltage-clamp recordings, the whole-cell current (I_w) flowing to ground through the resistance of the extracellular saline solution (of resistivity $\rho = 0.8\ \Omega\cdot m$) created a field potential (V_{fp}) that was largest at the cell surface and insignificant >100 μm away. Because the potential inside the focal pipette's tip was held at 0 mV, the potential difference across the seal resistance (R_s) equaled V_{fp}, and the current (I_{fp}) across the seal was $I_{fp} = V_{fp}/R_s$. To estimate I_{fp}, we assumed that I_w was distributed uniformly across the surface of a spherical cell; in this case, $I_{fp} = I_w R_c/R_s$, in which

$$R_c = \rho/(4\pi A)^{1/2} \tag{1}$$

is the convergence resistance to a sphere of surface area A (Hille, 1984). For an average-sized hair cell, for which $A = 1370\ \mu m^2$, $R_c = 6.1$ kΩ. During focal-current recordings, for which the average value of R_s was 1.6 MΩ and I_w was 2.1 nA, I_{fp} was therefore only 8 pA. I_{fp} had a time course identical to I_w; in effect, a small fraction (R_c/R_s) of the whole-cell current flowed to ground through the focal pipette, thereby contaminating the patch recording. To reduce the error due to I_{fp}, the equation above was used to estimate and subtract I_{fp} from each focal-current recording before calculation of the patch's capacitance and current density. This procedure eliminated the average contaminating current, producing a statistically unbiased estimate of the focal current density, but did not eliminate the effects of spatial nonuniformities in the extracellular field potential.

Most focal currents were averaged 100–1000 times to reduce the background (thermal) current noise across the seal resistance.

Capacitance measurements. The whole-cell capacitance was determined from dial settings on the voltage-clamp amplifier, which were adjusted to null the cell's capacitance and the electrode's resistance and capacitance. During focal recordings, the patch capacitance was determined from the time integral of the transient patch current in response to small voltage steps applied through the whole-cell pipette. The membrane areas of the patch and of the cell were then estimated assuming a specific membrane capacitance of 10 mF·m^{-2}.

Ensemble-variance analysis. The number, N, and single-channel current, i, of Ca^{2+} channels and Ca^{2+}-activated K^+ channels were determined from whole-cell voltage-clamp recordings by the ensemble-variance method (Sigworth, 1980). After isolating the current through either class of channels as described in Results, we presented trains of 102 identical, equally spaced voltage-step commands at 100-msec intervals. Interposed between these test stimuli, small voltage steps around the holding potential were presented, and the averaged response was stored for later use in leak subtraction. The responses to the first 2 test stimuli were discarded, and estimates of the mean, $m(t)$, and variance, $\sigma^2(t)$, of the whole-cell current were computed from the relations

$$m(t) = \frac{1}{K}\sum_{i=1}^{K} x_i(t), \tag{2}$$

$$\sigma^2(t) = \frac{1}{2(K-1)}\sum_{i=1}^{K-1} [x_i(t) - x_{i+1}(t)]^2, \tag{3}$$

in which $x_i(t)$ is the leak-subtracted response to the ith stimulus, and $K = 100$ is the number of stimuli used. The method used to estimate $\sigma^2(t)$ was designed to minimize the effects of "rundown," a gradual reduction in the response amplitude during stimulation, by averaging the squared differences between pairs of *consecutive* responses. Compared to the more straightforward procedure, in which $\sigma^2(t)$ is computed as the mean squared deviation from $m(t)$, this technique eliminated nearly all of the error due to rundown with only a modest (23%) increase in the standard error of the estimated $\sigma^2(t)$.

Using a maximum-likelihood procedure (W. M. Roberts, unpublished observations) that took into account how the error in $\sigma^2(t)$ varied as a function of t and $m(t)$, we estimated N and i by fitting parabolas to plots of $\sigma^2(t)$ versus $m(t)$. A least-squares fit was used to get initial estimates of N and i, which were used to compute the covariance of σ^2; $\mathrm{cov}(t_1, t_2) = E[\sigma^2(t_1)\sigma^2(t_2)] - E[\sigma^2(t_1)]E[\sigma^2(t_2)]$, in which E denotes an expected value. $\mathrm{cov}(t_1, t_2)$ describes the random deviations of $\sigma^2(t)$ from the expected parabolic dependence on $m(t)$, and was computed from the relation

$$\begin{aligned}\mathrm{cov}(t_1, t_2) = {} & [Ni^4C(t_1, t_2)/2(K-1)^2] \\ & \times [(6KN - 2K - 4N + 6)C(t_1, t_2) \\ & + (2K - 3)(2p(t_1) - 1)(2p(t_2) - 1)] \\ & + 3\sigma_n^4/(K-1),\end{aligned} \tag{4}$$

in which σ_n is the root-mean-square current noise when all channels are closed, $p(t) = m(t)/(Ni)$ is the probability that a single channel is open at time t, and $C(t_1, t_2)$ is the probability that a channel is open at times t_1 and t_2 (Roberts, unpublished observations). $C(t_1, t_2)$ was approximated by

$$C(t_1, t_2) = p(t_1)[p_\infty - p(t_2) + (1 - p_\infty)\exp(-|t_2 - t_1|/\tau)], \quad (5)$$

in which p_∞ and τ are, respectively, the asymptote and activation time constant determined by fitting a single-exponential curve to $p(t)$. Although neither Ca^{2+} channels nor Ca^{2+}-activated K^+ channels activate with a single-exponential time course in hair cells (Lewis and Hudspeth, 1983a; Ohmori, 1984; Art and Fettiplace, 1987; Hudspeth and Lewis, 1988a), this equation gave an adequate approximation to $C(t_1, t_2)$; for an exact formula based upon a fourth-order Hodgkin–Huxley model, see Conti et al. (1984).

The maximum-likelihood estimates of N and i were determined by an iterative procedure. At each stage, the old values of N and i were used to compute $\mathrm{cov}(t_1, t_2)$. Using a weighted, linear-least-squares procedure based on the Gauss–Markov theorem and the assumption that the noise in $m(t)$ is negligible (Roberts, 1979), we then computed new values of N and i from $\sigma^2(t)$, $m(t)$, and $\mathrm{cov}(t_1, t_2)$. The procedure was repeated until the new value of N differed from the previous value by $<1\%$. The maximum-likelihood procedure also gave estimates of the expected errors in N and i that were used to compute weighted averages of N and i when several stimulus trains were presented to the same cell.

Serial-section electron microscopy. Whole saccular maculae prepared as described previously (Kroese et al., 1989) were pinned out in a dish, and their otolithic membranes were removed without enzymatic digestion. The tissue was fixed for 1–2 hr at 4°C with 200 mM glutaraldehyde in 80 mM sodium cacodylate buffer (pH, 7.4) containing 5 mM $CaCl_2$. After a brief rinse in Ca^{2+}-containing buffer, the tissue was postfixed for 1 hr at 0°C with 40 mM OsO_4 in Ca^{2+}-containing buffer, rinsed again in the buffer solution, and dehydrated in a graded series of ethanol concentrations. The samples were stained *en bloc* for 1 hr at 4°C with 10 mM uranyl acetate in 95% ethanol, further dehydrated through absolute ethanol and propylene oxide, and embedded in epoxy plastic (EMbed 812, Electron Microscopy Sciences, Fort Washington, PA). Serial sections, cut at a thickness of 200 nm (Ultracut E ultramicrotome, Reichert-Jung, Vienna, Austria), were collected on Formvar-coated slot grids. The sections were examined and photographed without further staining in an electron microscope (JEM-100B, JEOL Ltd., Tokyo, Japan) operated at an accelerating voltage of 80 kV.

Freeze-fracture electron microscopy. Whole saccular maculae with intact otolithic membranes were subjected to 1 hr primary fixation as described above. After a brief rinse in Ca^{2+}-containing buffer solution, specimens were cryoprotected for 2 hr at 4°C with 23% glycerol in Ca^{2+}-containing buffer solution. Mounted in double-replica holders, the sacculi were then frozen by plunging into melting chlorodifluoromethane (Freon-22, DuPont, Wilmington, DE). At a temperature of −100°C and a pressure below 130 μPa, the tissue was fractured perpendicular to the epithelial surfaces in a freeze-fracture unit (BAF 400T, Balzers AG, Liechtenstein) equipped with a thin-film gauge. An electron-beam evaporation gun was then used to shadow the fractured surfaces with 5 nm platinum-carbon, half of which was applied with the specimen stage rotating. Samples were strengthened by carbon shadowing, removed from the vacuum, and rapidly warmed to room temperature. After residual tissue was dissolved with 30% household bleach, replicas were rinsed in distilled water and picked up on Formvar-coated grids. Replicas were examined and photographed in an electron microscope (JEM-100B, JEM-100C, or JEM-100SX, JEOL Ltd., Tokyo, Japan) operated at an accelerating voltage of 80 kV.

Results

Electrical resonance and whole-cell currents

Hair cells isolated from frog sacculi display a sharply tuned electrical resonance (Ashmore, 1983; Lewis and Hudspeth, 1983a; Hudspeth and Lewis, 1988a) that contributes importantly to their frequency selectivity *in vivo* (Crawford and Fettiplace, 1980, 1981). As in previous studies on other species (Lewis and Hudspeth, 1983a,b; Art and Fettiplace, 1987; Hudspeth and Lewis, 1988a), we found that 2 types of ion channels, voltage-gated Ca^{2+} channels and Ca^{2+}-activated K^+ channels, interact with each other and the membrane capacitance to create this resonance in hair cells from grass frogs.

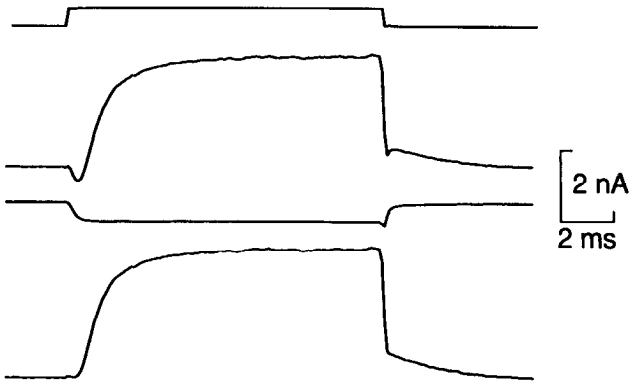

Figure 2. Separation of Ca^{2+} current from Ca^{2+}-activated K^+ current. A depolarizing voltage pulse from −70 to −20 mV (*first trace*) elicited a whole-cell current (*second trace*) with an inward transient followed by a sustained outward current. The Ca^{2+} current (*third trace*) was unmasked by moving the cell into a stream of extracellular saline solution that contained 20 mM TEA to block the Ca^{2+}-activated K^+ current. The K^+ current (*fourth trace*) was then obtained by subtraction of the 2 prior records.

As dictated by the objectives of specific experiments, we could separate the currents through the 2 types of channels by a combination of physiological and pharmacological techniques (Fig. 2). To record whole-cell Ca^{2+} currents in isolation, we could block all K^+ currents by perfusing a cell with Cs^+-aspartate internal solution (Table 1). The Ca^{2+} current could also be isolated by immersing a cell in solution containing tetraethylammonium ion (TEA). The Ca^{2+}-activated K^+ current could then be determined by subtracting the Ca^{2+} current from the total current in the absence of TEA. A third current, the transient K^+ current (A-current), is not essential for electrical resonance; this current could be inactivated by holding the membrane potential at −65 to −70 mV (Lewis and Hudspeth, 1983a; Hudspeth and Lewis, 1988a).

The number of Ca^{2+} channels per hair cell

To estimate the number of Ca^{2+} channels (N_{Ca}) and their single-channel currents (i_{Ca}), we used a Ca^{2+}-channel agonist, the dihydropyridine (+)202791 (Perney et al., 1986), to increase the channels' open probability and slow their deactivation rate. After a 15-min bath perfusion with saline solution containing 5 μM (+)202791, a conspicuous, slowly decaying tail current was apparent when the potential was restored to −65 mV following a brief depolarization that opened most Ca^{2+} channels (Fig. 3*A*). Because of the large driving force on Ca^{2+} at the holding potential, the current noise during such tail currents was large enough for estimation of both N_{Ca} and i_{Ca} (Fig. 3*B,C*). The mean current and variance were computed from trains of 100 stimuli, each of which comprised 3 2–4-msec depolarizations separated by 4–6-msec hyperpolarizations to −65 mV. The duration of each voltage pulse was made just long enough for the current to reach a steady state. Separate estimates of N_{Ca} and i_{Ca} were computed from the tail currents during each of the 3 hyperpolarized portions of the stimulus; the current during the initial 1 msec after each hyperpolarizing command was excluded from the analysis because the voltage had not yet stabilized. The 3 estimates were averaged after weighting each by its calculated variance. Each

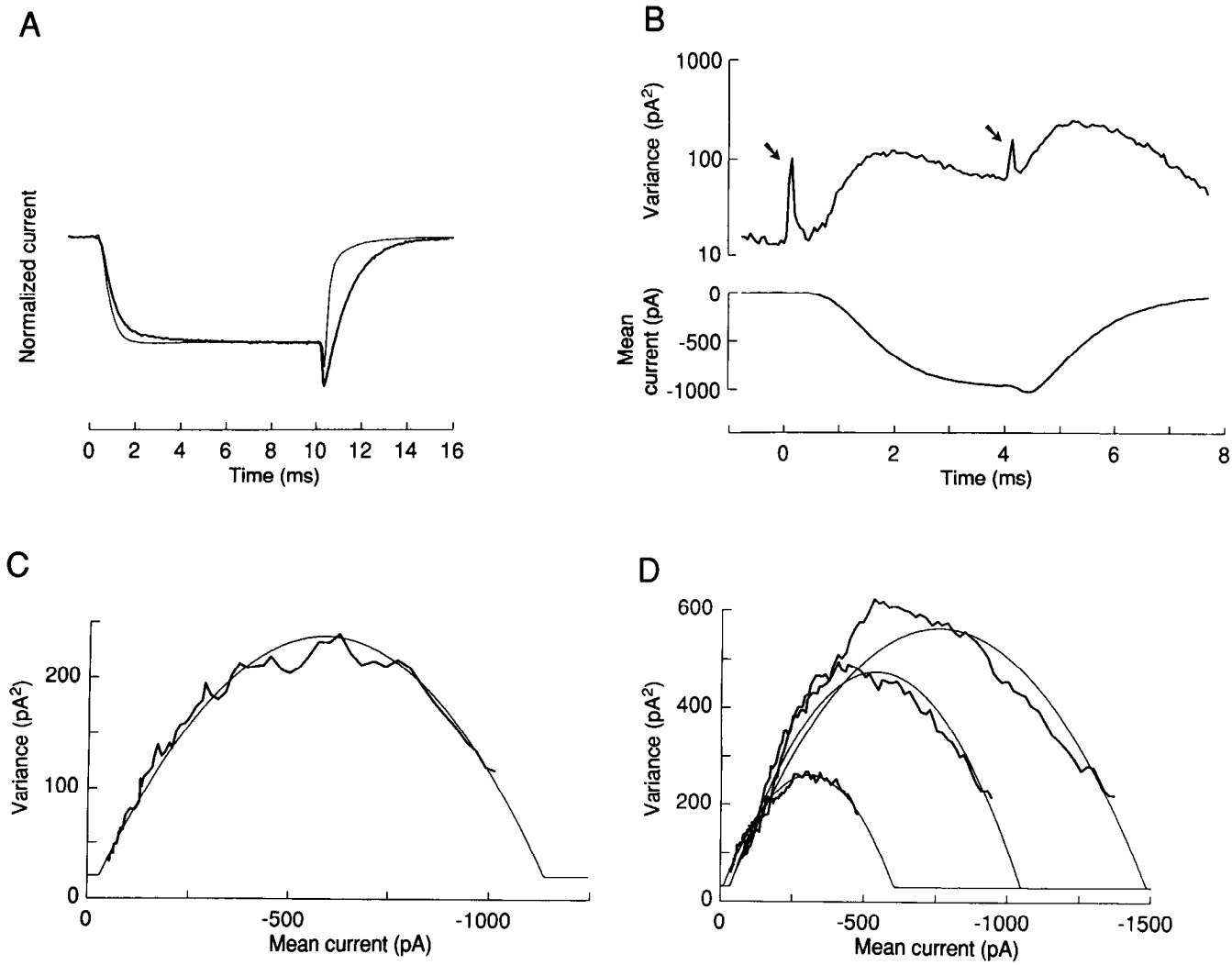

Figure 3. Ensemble-variance analysis of Ca^{2+} current with Cs^+-aspartate internal solution to block Ca^{2+}-activated K^+ current. *A*, Normalized Ca^{2+} currents from 2 cells during voltage-clamp pulses from −65 to −20 mV. The *thin trace* was recorded before, and the *thick trace* after, perfusion of the bath with 5 μM of the dihydropyridine (+)202791; the peak currents were, respectively, −820 pA and −1420 pA. The most obvious effect of the drug was to prolong the tail current after repolarization to −65 mV; the decay time constants were 300 μsec before and 1050 μsec after addition of the drug. *B*, Mean and variance of the Ca^{2+} current in another cell (cell 1 in Table 2) with (+)202791 in the bath. *Traces* are averages of 300 stimuli; *arrows* indicate artifacts at the onset and termination of depolarization from −65 to −32 mV. An increased variance is evident as the Ca^{2+} current commences, as well as during the tail current. Note the logarithmic variance scale. *C*, Plot of variance versus mean from the Ca^{2+} tail current in *B*. The smooth parabola, calculated by a maximum-likelihood procedure, corresponds to estimates of N_{Ca} = 1409 ± 100 and i_{Ca} = −0.79 ± 0.05 pA. The background variance of 20 pA^2 is indicated by the *flat portions* of the *fitted curve*; the maximum-likelihood algorithm was not constrained to fit the data to a curve through the origin. *D*, Fits of data from tail currents taken at 3 times after initiating whole-cell recording (cell 2 in Table 2) demonstrate that, during rundown of the Ca^{2+} current, N_{Ca} decreased while i_{Ca} remained unchanged. Fitted values of N_{Ca} and i_{Ca} are N_{Ca} = 990, i_{Ca} = −1.47 pA at 119 sec; N_{Ca} = 577, i_{Ca} = −1.75 pA at 152 sec; and N_{Ca} = 380, i_{Ca} = −1.56 pA at 185 sec. The values of N_{Ca} and i_{Ca} shown in *C* and *D* were obtained from single fits to means and variances averaged from responses to 300 stimuli and thus differ somewhat from the values given for the same cells in Table 2, which were averaged from 3 separate fits to 100-stimulus segments of data.

value of N_{Ca} and i_{Ca} was thus determined from the noise recorded during 300 tail currents.

Most cells remained healthy long enough to permit several repetitions of the train of 100 test stimuli with an interval of ~20 sec between trains. In some cells, the Ca^{2+} current showed a steady decline in amplitude, or rundown, during this period. Analysis of records taken at various times after breaking into such a cell indicated that rundown was due to a decline in N_{Ca} without a significant change in i_{Ca} (Fig. 3*D*).

Because rundown was associated with a decline in N_{Ca}, we used only the values computed from the first stimulus train to calculate the average number of Ca^{2+} channels per cell. Data from 6 cells are shown in Table 2. Statistical analysis demonstrated that the variability between cells was larger than the error in determining N_{Ca} in a given cell, so equal weight was given to each of the 6 values to compute the overall mean value of 1800 ± 400 Ca^{2+} channels per cell (mean ± SEM, 2 significant digits).

Because the single-channel current did not appear to change during rundown, we used data from all the tail currents recorded in the same 6 cells to calculate an average single-channel Ca^{2+} current of −1.2 ± 0.2 pA at a holding potential of −65 mV

Table 2. Variance analysis of Ca^{2+} channels

Cell number	N_{Ca} mean ± SEM (*n*)	i_{Ca} (pA) at −65 mV mean ± SEM (*n*)	Time (sec)
1	2121 ± 294 (3)	−0.75 ± 0.03 (18)	375
2	1018 ± 44 (3)	−1.48 ± 0.04 (15)	119
3	770 ± 86 (3)	−1.77 ± 0.09 (15)	65
4	2780 ± 410 (3)	−0.82 ± 0.03 (21)	8
5	984 ± 149 (3)	−1.61 ± 0.07 (18)	26
6	3101 ± 459 (3)	−0.78 ± 0.04 (12)	13
	1796 ± 412 (6)	−1.20 ± 0.19 (6)	

The properties of Ca^{2+} channels were determined by ensemble-variance analysis of tail currents with 5 μM of the dihydropyridine (+)202791 in the bath and Cs^+-aspartate internal solution in the whole-cell pipette. N_{Ca} is the number of channels per cell; i_{Ca} is the single-channel current. Times were measured from breaking into the cell to the beginning of the first stimulus train. Each train lasted ~10 sec and produced 3 independent fits of N_{Ca} and i_{Ca}. Approximately 30 sec elapsed from the onset of one train to the beginning of the next. The average values of N_{Ca} and i_{Ca} given for each cell are weighted means from *n* independent maximum-likelihood fits, each of which was based upon the current's mean and variance calculated from responses to 100 stimuli. The grand means are equally weighted averages of the means from the 6 cells.

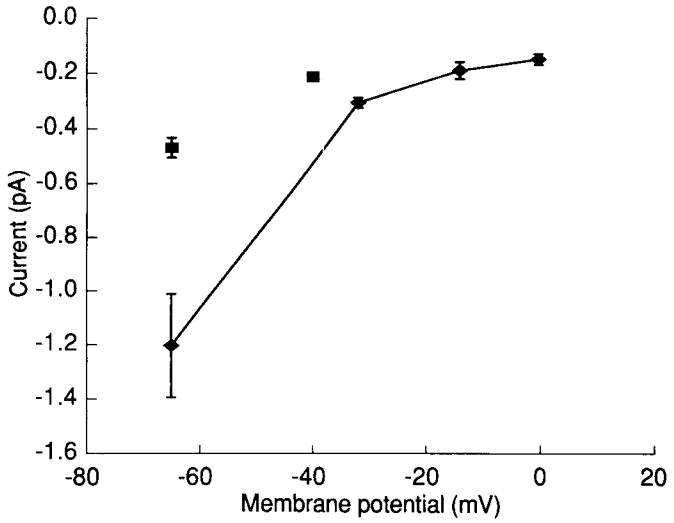

Figure 4. Single-channel Ca^{2+} currents estimated from ensemble-variance analysis with (*diamonds*) and without (*squares*) the dihydropyridine (+)202791 in bath. The SEMs are shown if larger than the symbols. See the text for details of the procedure.

(Fig. 4, diamond symbol at −65 mV). As with estimates of N_{Ca}, the variation among estimates of i_{Ca} obtained from the same cell was much less than the variation among cells (Table 2).

In 3 cells, the baseline current noise was small enough that noise analysis could be performed during the depolarized portions of the stimulus trains, for which i_{Ca} was smaller than at −65 mV (Fig. 3*B*). Averaged values of i_{Ca} from these cells are shown in Figure 4 (diamond symbols at −32, −14, and 0 mV).

Even in the absence of dihydropyridines, depolarizations to potentials between −20 mV and −50 mV resulted in single-channel currents large enough to be determined from the initial slopes of mean-variance plots (Fig. 4, square symbol at −40 mV). The steady-state open probability at these potentials was too small, however, for determination of the number of Ca^{2+} channels. The single-channel current at the holding potential was estimated from noise measurements during tail currents (Fig. 4, square symbol at −65 mV). These measurements probably provided an underestimate of i_{Ca}; without the dihydropyridine agonist to prolong channel openings, a substantial part of the current noise lay outside the passband of our recording circuit.

The number of Ca^{2+}-activated K^+ channels per hair cell

The large single-channel conductance of the hair cell's Ca^{2+}-activated K^+ channels facilitates the observation of current noise associated with their random opening and closing (Art and Fettiplace, 1987; Hudspeth and Lewis, 1988a), but the channels' Ca^{2+} dependence complicates the analysis of K^+-current noise for 2 reasons. First, the K^+ current is not ordinarily observed in isolation from the Ca^{2+} current, which provides the influx of Ca^{2+} needed to open the K^+ channels. Second, spatial variations in the intracellular concentration of free Ca^{2+} ($[Ca^{2+}]_i$) might negate the crucial assumption for ensemble-variance analysis, that all Ca^{2+}-activated K^+ channels have identical open probabilities.

These 2 difficulties were eliminated by cytoplasmic dialysis with pipette solutions containing known, buffered concentrations of free Ca^{2+}. Dialysis with internal solution containing 66 mM BAPTA and <1 nM free Ca^{2+} did not prevent the activation of K^+ channels unless the Ca^{2+} current was also blocked (Fig. 5*A*); the influx of Ca^{2+} was sufficient to saturate even isotonic BAPTA in the vicinity of the Ca^{2+}-activated K^+ channels. Most buffered-Ca^{2+} experiments accordingly were performed with the Ca^{2+} current blocked by 10 mM Co^{2+} in the bath. A $[Ca^{2+}]_i$ of 5 μM or greater caused the Ca^{2+}-activated K^+ channels to open upon depolarization without the usual delay (Fig. 5*B*), a result consistent with the suggestion that the channels' time course of activation is normally limited by the diffusion and binding of Ca^{2+} ions and the initial, Ca^{2+}-dependent conformational changes in the K^+-channel protein (Hudspeth and Lewis, 1988a).

To determine the time required for equilibration of the intracellular Ca^{2+} concentration, we recorded Ca^{2+}-activated K^+ currents during the initial 120 sec after breaking into a cell. With the Ca^{2+} current blocked and a free $[Ca^{2+}]_i$ of <10 μM in the internal solution, current–voltage relations indicated that the Ca^{2+} concentration initially exceeded 1 mM (see below), then declined to a steady value during the subsequent 10–60 sec (data not shown). This result suggests that Ca^{2+} diffused out of the pipette faster than Br_2BAPTA, which has a relative molecular mass of 944 Da. All analyses were accordingly conducted after waiting at least 70 sec for the intracellular Ca^{2+} concentration to equilibrate with that in the pipette.

Ensemble-variance analysis was used to determine the number of Ca^{2+}-activated K^+ channels that were active under these conditions of buffered $[Ca^{2+}]_i$. As for Ca^{2+} channels, values of N_K and i_K were computed from maximum-likelihood fits to the mean and variance data collected during trains of 100 stimuli presented in a ~10-sec interval (Fig. 5*C,D*). Data were collected during substantial depolarizations, to potentials between +20 and +70 mV, at which the single-channel current was large and the steady-state open probability exceeded 80%. When possible, several trains were presented, and the data from each were analyzed separately to produce multiple estimates of N_K and i_K for each cell (Table 3). Because rundown of the Ca^{2+}-activated K^+ current was not apparent, all values of N_K were used to compute the mean number of channels in each cell. These values were then averaged to give an overall mean estimate of 550 ±

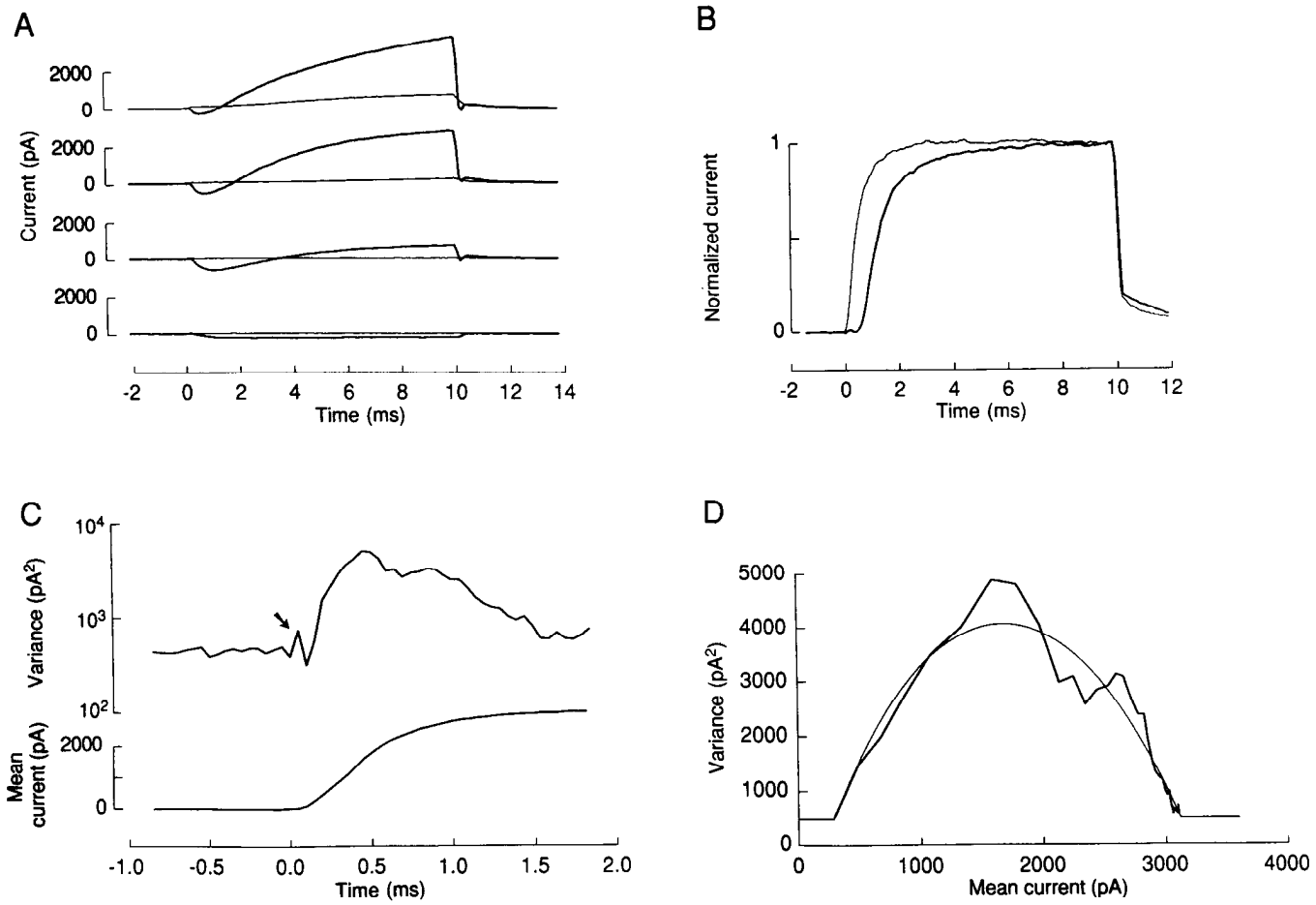

Figure 5. Analysis of Ca^{2+}-activated K^+ currents with buffered internal Ca^{2+} concentrations. *A*, With an internal solution containing 66 mM BAPTA and nominally <1 nM free Ca^{2+}, the cell's Ca^{2+} current was nevertheless sufficient to activate the K^+ current at potentials positive to −40 mV (*thick traces*). The Ca^{2+}-activated K^+ current was suppressed by blocking the Ca^{2+} current with 10 mM Co^{2+} added to the bath (*thin traces*). Depolarizations were to (from *top* to *bottom*) +20, 0, −20, and −40 mV. BAPTA was able to block the Ca^{2+}-activated K^+ current at −40 mV, but merely slowed the activation rate at more depolarized potentials. We did not determine the source of the small outward current that remained after adding Co^{2+}. The *thick* and *thin traces* were obtained from 2 different cells. *B*, After blockage of the Ca^{2+} current and perfusion with an internal solution containing 5 μM free Ca^{2+}, depolarizing steps evoked an outward current with an exponentially rising time course (*thin trace*), without the delay normally seen when the K^+ current was activated by the cell's Ca^{2+} current with K^+-aspartate internal solution (*thick trace*). Data were taken from 2 different cells upon depolarization to −20 mV. *C*, Ensemble mean and variance averaged from 100 steps to +45 mV (cell 1 in Table 3). The *arrow* marks an artifact at the step's onset. *D*, From this maximum-likelihood fit to the data from *C*, we estimated values of $N_K = 568$ and $i_K = 5.0$ pA.

70 Ca^{2+}-activated K^+ channels per cell (mean ± SEM, 2 significant digits).

Table 3 also gives values for the single-channel K^+ current. To facilitate averaging of single-channel current measurements collected at different depolarized potentials and with different free K^+ concentrations (see Table 1), we converted all single-channel currents as described below to the equivalent current (i_0) under standard conditions of 0 mV membrane potential and 104 mM free intracellular K^+ concentration. To correct for differences in membrane potential, we determined the open-channel current–voltage relation (Fig. 6*A*) from the ratio of the steady-state current at a given potential to the size of the tail current upon repolarization to −40 mV, then used the fitted curve shown in Figure 6*A* to convert single-channel currents measured at potentials between +25 and +70 mV to the equivalent currents at 0 mV. We corrected for differences in the free $[K^+]_i$ by assuming that i_0 was proportional to the free K^+ concentration. The values of free K^+ concentration in the internal and external saline solutions given in Table 1 were consistent with the reversal potential for the K^+ tail current (Fig. 6*A*, data point at −93 mV).

By analysis of tail currents, we determined the voltage dependence of K^+-channel opening under conditions of constant $[Ca^{2+}]_i$, as well as in response to the cell's Ca^{2+} current (Fig. 6*B*). At a constant $[Ca^{2+}]_i$, the K^+ channel's open probability was only weakly voltage dependent; the Boltzmann slope coefficient was 26 mV. As with other Ca^{2+}-activated K^+ channels, increasing the $[Ca^{2+}]_i$ shifted the voltage dependence of the channel's open probability such that the channel opened at more negative potentials. The much steeper voltage dependence in response to the cell's Ca^{2+} current indicates that most of the K^+ current's apparent voltage sensitivity results from changes in $[Ca^{2+}]_i$ that ensue upon depolarization.

From the voltages at which the steep curve crossed the 3 shallow curves in Figure 6*B*, we estimated that the steady-state local $[Ca^{2+}]_i$ at the K^+ channel's Ca^{2+}-binding site was 10 μM at −58 mV, 100 μM at −53 mV, and 1 mM at −42 mV. At potentials between −42 and +15 mV, the steady-state local

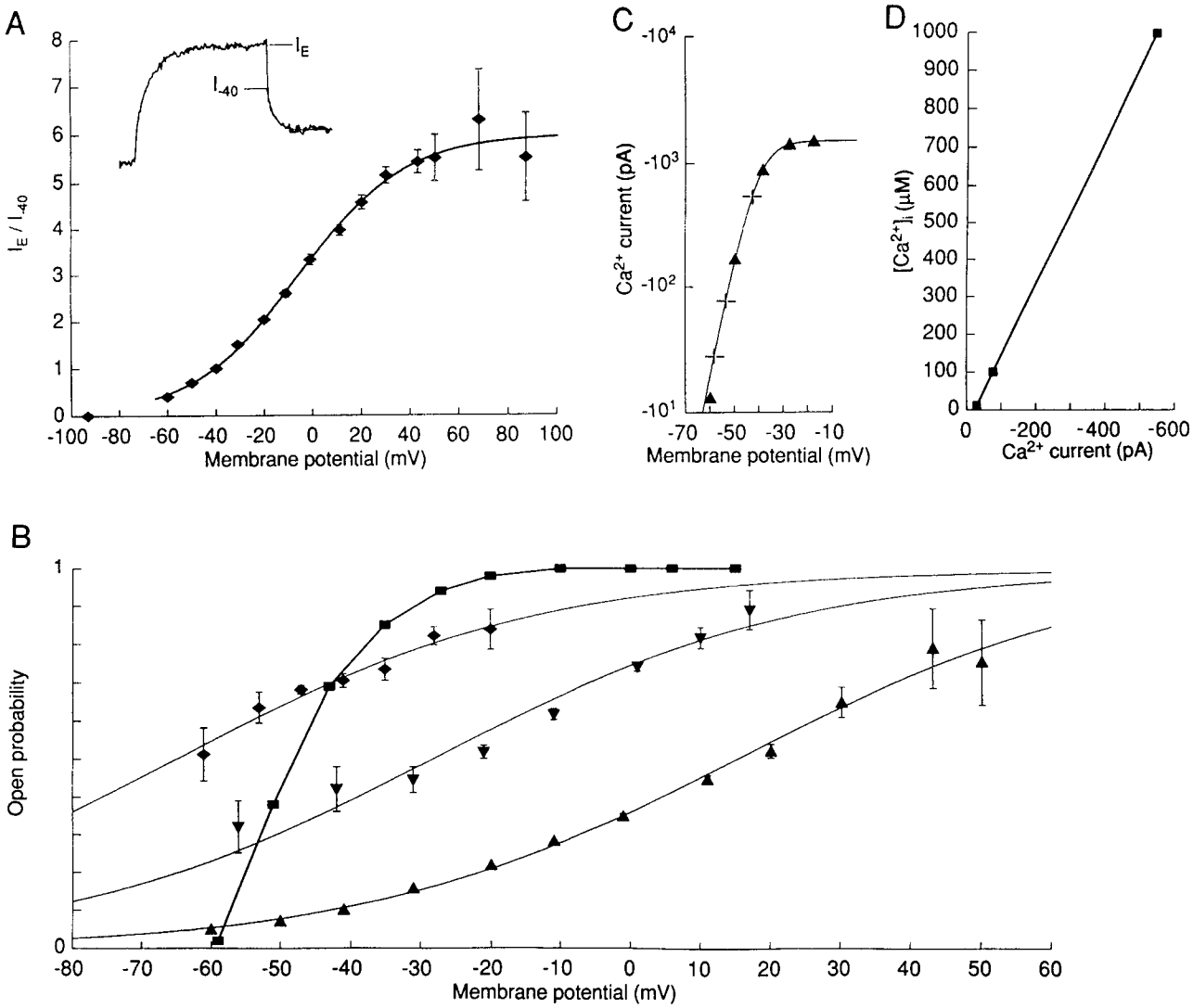

Figure 6. *A,* The current–voltage relation of an open Ca^{2+}-activated K^+ channel, determined from whole-cell recordings. We blocked the Ca^{2+} current and recorded K^+ currents in the presence of 10 μM free $[Ca^{2+}]_i$. For each *data point,* we stepped the membrane potential between 2 levels (E and −40 mV) and determined the K^+ current before (I_E) and after (I_{-40}) the step. I_{-40} was measured by fitting the tail current with a single exponential relation and extrapolating back to the onset of the step (*inset*). Because I_E and I_{-40} represent currents through the same number of open channels at 2 different potentials, their ratio is independent of this number; I_E/I_{-40} is accordingly plotted against E. A sigmoidal curve was fit to the data for use in *B* of this figure and in Table 3. *B,* The weak voltage dependence of K^+ channel opening in buffered, constant $[Ca^{2+}]_i$ (*triangles,* 10 μM; *inverted triangles,* 100 μM; *diamonds,* 1 mM) with the Ca^{2+} current blocked contrasts with its steep dependence during activation by the cell's Ca^{2+} current (*squares*). We measured tail-current amplitudes at −40 mV following voltage-clamp steps to the potentials indicated along the *abscissa.* Before the data from different cells were averaged, variations between cells were reduced by normalizing to the tail current's amplitude following a step to 0 mV (*triangles, inverted triangles, squares*) or to −45 mV (*diamonds*). The sigmoidal curves are weighted, least-squares fits to the equation $y = a/\{1 + \exp[-(E - E_h)/b]\}$. The curve for 10 μM $[Ca^{2+}]_i$ yields the best fit of all 3 parameters; $a = 2.8$, $E_h = 15$ mV, and $b = 26$ mV. Because the data for 100 μM and 1 mM $[Ca^{2+}]_i$ did not encompass a sufficient voltage range to constrain the values of all 3 parameters, we assumed that the voltage sensitivity ($b = 26$ mV) was independent of $[Ca^{2+}]_i$ (Hudspeth and Lewis, 1988a) and fit the remaining 2 parameters ($a = 1.35$, $E_h = -28$ mV at 100 μM; $a = 1.44$, $E_h = -65$ mV at 1 mM). Each curve and the associated *data points* are plotted as fractions of the asymptotic maxima (*triangles, inverted triangles, diamonds*) or of the actual maximum (*squares*). The measurements made in 100 μM and 1 mM $[Ca^{2+}]_i$ differed from those made in 10 μM $[Ca^{2+}]_i$ in 2 additional respects. First, because the higher concentrations of free Ca^{2+} opened a significant fraction of the K^+ channels at the holding potential (−70 mV), leak subtraction was not used. Second, we did not directly measure tail currents, but inferred them by dividing steady-state currents at the potentials indicated by the current–voltage relation given in *A. C,* The voltage dependence of the Ca^{2+} current was determined from steady-state Ca^{2+} currents (*triangles*) recorded after blocking the K^+ current. The *crosses* are placed on the fitted curve at the voltages at which the 3 constant-$[Ca^{2+}]_i$ curves in *B* cross the fourth curve. The values on the *ordinate* that correspond to these 3 intersections give the approximate Ca^{2+} currents that produce $[Ca^{2+}]_i$ values of 10 μM, 100 μM, and 1 mM at the K^+ channels' binding sites. *D,* The $[Ca^{2+}]_i$ values are plotted against the Ca^{2+} currents derived in *C* to show the approximately linear relation between the whole-cell Ca^{2+} current and $[Ca^{2+}]_i$, with a slope of −1.8 mM/pA. In *A* and *B, triangles, inverted triangles,* and *diamonds,* the internal solution contained 40 mM Br_2BAPTA; 10 mM Co^{2+} was added to the external solution. The internal solution was K^+-aspartate for *B, squares,* and Cs^+-aspartate in *C.* Each *data point* in *A* and *B* is the mean of: *A,* 3–19 cells; *B,* 15 (*triangles*), 7 (*inverted triangles*), 5 (*diamonds*), or 4 (*squares*) cells. SEMs are shown when larger than the symbols.

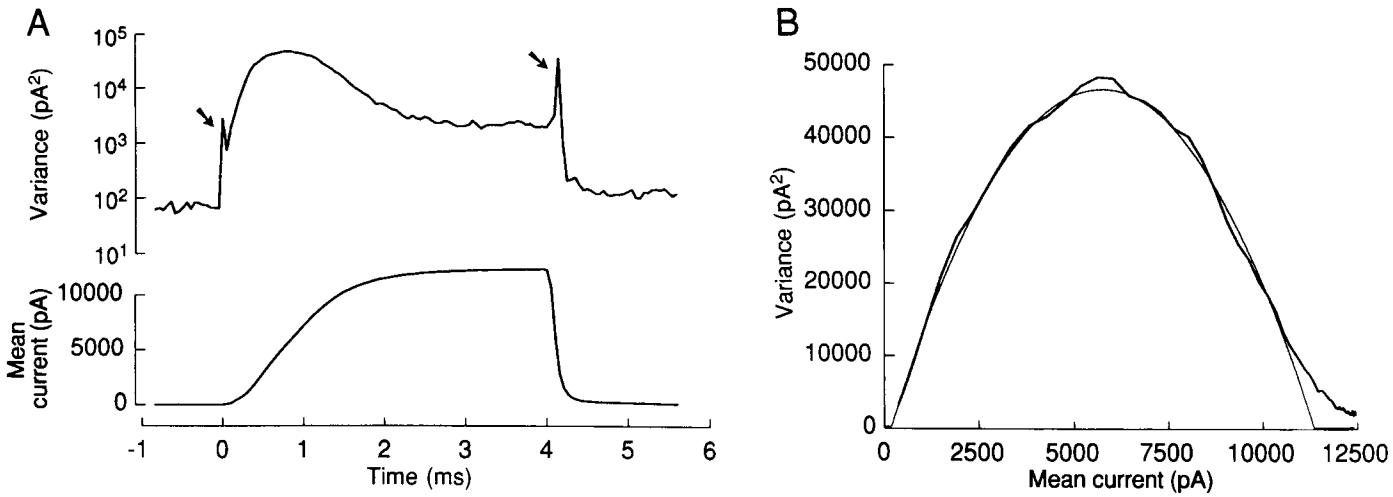

Figure 7. Analysis of Ca^{2+}-activated K^+ channels activated by cell's Ca^{2+} current. *A*, Mean and variance during a voltage pulse from −70 to +50 mV; average of 200 responses (cell 17 in Table 3). The *arrows* mark artifacts at the pulse's onset and termination. *B*, Maximum-likelihood fit to the data in *A*; $N_K = 671$, $i_K = 16.6$ pA, and $i_0 = 10.1$ pA. Because the data deviated from the predicted parabolic curve at later times, only data obtained during the first 1.5 msec were used to fit N_K and i_K.

$[Ca^{2+}]_i$ apparently exceeded 1 mM. We then used the Ca^{2+} current's known voltage sensitivity (Fig. 6*C*) to convert the dependence of the local $[Ca^{2+}]_i$ on membrane potential to its dependence on the size of the Ca^{2+} current (Fig. 6*D*). The relation was approximately linear, with a slope of 1.8 μM/pA.

If Ca^{2+} entry through a hair cell's Ca^{2+} channels creates large spatial gradients in $[Ca^{2+}]_i$, it is possible that the population of Ca^{2+}-activated K^+ channels active under conditions of uniformly high $[Ca^{2+}]_i$ included channels that were usually inactive because they were located in regions where $[Ca^{2+}]_i$ was ordinarily low. To exclude this possibility, we performed ensemble-variance analysis using the cell's Ca^{2+} current to provide the requisite Ca^{2+} ions. Although depolarization to any potential positive to −50 mV caused obvious current noise associated with the opening of K^+ channels (Art and Fettiplace, 1987; Hudspeth and Lewis, 1988a), we restricted our quantitative analysis to K^+-current noise during large depolarizations to potentials between +25 and +65 mV, at which the Ca^{2+} current was much reduced from its peak near −10 mV and thus added negligible noise and only a small current to the much larger Ca^{2+}-activated K^+ current. An additional benefit of using large depolarizations was the slow activation of the K^+ current that resulted from the small size of the Ca^{2+} current (Hudspeth and Lewis, 1988a).

Figure 7 illustrates the noise analysis for the Ca^{2+}-activated K^+ current evoked by 100 stimuli presented to 1 cell. The peak variance at +50 mV was ~500-fold as large as the background variance at −70 mV (Fig. 7*A*) and had the expected parabolic dependence on the mean current during the initial ~1.5 msec after the depolarization's onset (Fig. 7*B*). The data from most cells studied under these conditions deviated from the parabolic relation at later times, possibly because of a small contaminating current. To minimize the effects of this contamination, we determined maximum-likelihood values for N_K and i_K by analyzing the mean-variance data during the initial 1.5 msec of the step. The estimates of 820 ± 80 K^+ channels per cell and of a unitary conductance of 7.0 ± 1.0 pS (means ± SEMs, 2 significant digits; Table 3), which are in reasonable agreement with the values obtained in the presence of buffered $[Ca^{2+}]_i$, indicate that a cell's Ca^{2+} current can open essentially all of the cell's Ca^{2+}-activated K^+ channels.

Spatial distribution of ion channels

We mapped channel distributions by using loosely sealed pipettes to record from membrane patches of known size and location on the cellular surface while applying voltage pulses and recording the total membrane current through a whole-cell pipette. The whole-cell voltage clamp was necessary for 2 reasons. First, in contrast to previous loose-seal mapping studies on muscle cells (Stühmer et al., 1983; Roberts, 1987), the intracellular potential was neither known a priori nor necessarily constant; these hair cells had a high resting input resistance (~1 GΩ) that made the membrane potential susceptible to perturbation by focal currents of only a few picoamperes. Second, without a means of applying voltage pulses intracellularly, it would have been necessary to apply them through the focal electrode, and leak subtraction would have been required to separate patch currents from leakage across the seal. Artifacts inherent in leak subtraction would then have obscured the small patch currents recorded in these experiments. We recorded both focal and whole-cell currents so that we could express each focal current as a fraction of the whole-cell current and thus eliminate the possibility that patches deficient in ionic currents reflected poor physiological condition of the cells.

The apical membrane surface lacks voltage-gated ion channels

To compare the populations of ion channels on the apical and basolateral membrane surfaces, we used a large (~10-μm-diameter), loosely sealed pipette to record from the entire apical surface, including the hair bundle (Fig. 1*C*). The basolateral current was determined by subtracting the apical current from the whole-cell current. Neither depolarizing steps, which evoked large whole-cell Ca^{2+} and K^+ currents, nor hyperpolarizing steps, which yielded inward currents through inwardly rectifying K^+ channels (data not shown; Corey and Hudspeth, 1979a; Ohmori, 1984), elicited measurable voltage-gated currents from the apical surface (Fig. 8).

Cable properties of stereocilia

Although we found no evidence of voltage-gated ion channels on the apical cellular surface, we did record large capacitive

Table 3. Variance analysis of Ca^{2+}-activated K^+ channels

Cell number	N_K mean ± SEM (n)	i_O (pA) mean ± SEM (n)	Time (sec)	Ca^{2+} concentration (μM)
With buffered intracellular Ca^{2+} concentrations				
1	620 ± 91 (18)	3.0 ± 0.3 (18)	99	1000
2	455 ± 99 (9)	5.0 ± 0.9 (9)	111	1000
3	423 ± 93 (3)	4.1 ± 0.4 (3)	133	1000
4	408 ± 91 (3)	5.5 ± 0.9 (3)	109	1000
5	365 ± 94 (6)	5.8 ± 0.7 (6)	101	1000
6	955 ± 126 (20)	6.2 ± 0.5 (20)	153	10
7	549 ± 158 (10)	3.2 ± 0.4 (10)	79	1
8	638 ± 421 (7)	5.1 ± 1.7 (7)	200	1
	552 ± 68 (8)	4.7 ± 0.4 (8)		
Activated by the cell's Ca^{2+} current				
9	929 ± 83 (4)	6.3 ± 0.5 (4)	88	
10	850 ± 91 (3)	9.1 ± 0.8 (3)	75	
11	962 ± 171 (2)	4.7 ± 0.7 (2)	82	
12	1042 ± 171 (2)	4.2 ± 0.6 (2)	81	
13	829 ± 83 (4)	5.7 ± 0.5 (4)	173	
14	1349 ± 157 (4)	4.0 ± 0.4 (4)	81	
15	803 ± 129 (3)	4.9 ± 0.7 (3)	79	
16	390 ± 37 (4)	14.8 ± 1.2 (4)	85	
17	634 ± 27 (10)	6.9 ± 0.3 (10)	101	
18	586 ± 91 (1)	10.5 ± 1.4 (1)	78	
19	608 ± 110 (1)	6.1 ± 1.1 (1)	187	
	816 ± 79 (11)	7.0 ± 1.0 (11)		

The properties of Ca^{2+}-activated K^+ channels were determined by ensemble-variance analysis. N_K is the number of channels per cell and i_0 is the single-channel current at a membrane potential of 0 mV (see text). Times were measured from breaking into a cell to the beginning of the first stimulus train. Each train lasted ~10 sec and produced 1–3 independent fits of N_K and i_0. Buffering of the intracellular Ca^{2+} concentration is described in the text. Calculations of means and SEs were carried out as for Table 2.

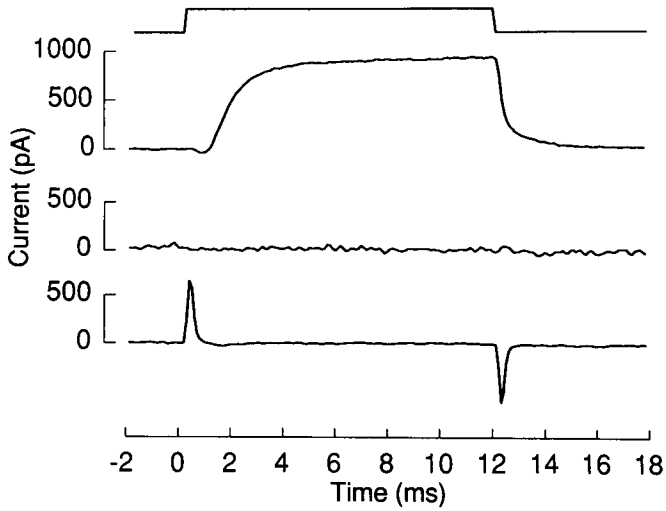

Figure 8. During a depolarization from −70 to −20 mV (*first trace*), a tightly sealed electrode measured a hair cell's whole-cell current (*second trace*). At the same time, a large, loosely sealed pipette covering the entire apical surface recorded the apical-membrane current (*third trace*). The 2 *middle traces* and the focal-current records in all other figures were subjected to leak subtraction; the *fourth trace* displays the apical current without leak subtraction to demonstrate the capacitive current. An exponential fit to the declining phase of the capacitive transient gave a time constant of 110 μsec; the *area beneath* the transient corresponded to an apical membrane capacitance of 4.0 pF.

currents (Fig. 8, fourth trace). We studied these transients in order to verify an important corollary of our model for mechanoelectrical transduction (Hudspeth, 1982; Howard et al., 1988), that receptor currents generated at the stereociliary tips can flow with negligible loss into the cell body. From the area beneath the charging transient, we first determined that the average apical membrane capacitance is 4.0 ± 0.3 pF (mean ± SEM, 7 cells). This is a substantial fraction of the total cellular capacitance of 13.7 ± 0.3 pF (mean ± SEM, 77 cells); the apical membrane includes ~30% of a hair cell's surface area. The specific capacitance of lipid-bilayer membranes is almost always 10 $mF \cdot m^{-2}$. The large apical capacitance could therefore be produced by 400 μm^2 of membrane that experienced the full voltage change applied at the cell body, but would require a larger membrane area if the voltage were substantially attenuated as it spread along the stereocilia. The apical surface area determined by morphometry, ~460 μm^2 (Table 4), only slightly exceeded the physiologically established minimum, from which we conclude that the voltage reached the stereociliary tips with little decrement.

To estimate the maximal internal resistivity of stereocilia, we next compared the apical capacitive currents to the results derived from an electrical model of the hair bundle. We assumed that the bundle consisted of 63 cylindrical, 300-nm-diameter stereocilia with the distribution of lengths described in the legend to Table 4. The membrane capacitance was calculated from the stereociliary surface areas, and the membrane resistance was estimated by apportioning the measured apical leakage conductance, 180 ± 140 pS (mean ± SEM, 7 cells), equally among the stereocilia. This conductance was so small that our results were not significantly affected by distributing the leak uniformly along the stereocilia, concentrating it at the stereociliary tips, or ignoring it altogether.

We employed cable equations in which the only unknown parameter value was the internal resistivity of the actin-packed stereociliary cytoplasm. Increasing this resistivity slowed the charging transients in the simulations. We quantified this effect by fitting an exponential relation to the declining phase of the transient current over the interval 100–900 μsec after the voltage step. We employed the same fitting procedure on recorded and simulated data and used the resultant time constants as a basis of comparison.

Because the time constants of recorded transients were usually <200 μsec, near the limit imposed by the speed of our voltage-clamp system, they were overestimates of the time constants that would have followed instantaneous voltage changes. We therefore used the smallest value, 110 μsec (Fig. 8), for comparison with model simulations. The largest internal resistivity compatible with a time constant of 110 μsec was 35 Ω·m. For a stereocilium 6.7 μm in length, the average in these cells, the end-to-end conductance exceeds 300 pS. It is possible that a significant part of a stereocilium's internal resistance is concentrated in the tapered region at its base; we found that including such a resistance in the simulation *decreased* the maximum possible resistance between the stereocilium's tip and base, however, and this possibility could therefore be ignored in these calculations.

A steady receptor current generated by a membrane conductance change at the tip of a stereocilium will be attenuated only

Table 4. Membrane area of the apical cellular surface

Measurement number	Number of stereocilia	Longest stereocilium (μm)	Shortest stereocilium (μm)	Mean interciliary spacing (μm)	Apical diameter (μm)
1	67*	9.4	4.6	0.67	9.0
2	58*	9.2	3.6	0.69	9.4
3	60*	9.2	4.8	0.70	8.8
4	62*	9.8	4.0	0.70	9.4
5	66*	9.4	3.6	0.69	9.8
6	64*	8.8	3.8	0.73	10.2
7	62*	9.4	4.0	0.69	10.4
8	63*	8.6	3.8	0.70	10.0
9	63*	9.2	4.0	0.67*	8.8
10	66*	9.7*	4.7*	0.67*	9.8
11	61*	10.0*	4.7*	0.71*	8.8
12	64*	9.3*	4.0*	0.71*	9.6
13	—	9.3*	5.0*	0.67*	—
	63 ± 1	9.3 ± 0.1	4.2 ± 0.1	0.69 ± 0.01	9.5 ± 0.2

The measurements, calibrated against a 10-μm stage micrometer (Carl Zeiss, Oberkochen, FRG), were made on hair cells prepared by 2 means. Most dimensions were obtained from differential-interference-contrast photomicrographs of enzymatically isolated, living hair cells. The data marked by asterisks were instead taken from photomicrographs of toluidine blue-stained, 500-nm-thick sections of glutaraldehyde-fixed, plastic-embedded hair cells prepared as described in Materials and Methods. Except for the second and third data columns, the measurements in each column were taken from different cells; each final value is reported as mean ± SEM. Each value for interciliary spacing is the mean measured along a row of 6–9 stereocilia in a bundle's plane of bilateral symmetry. The hair bundle of a large cell, typical of those used in the physiological recordings, includes 63 stereocilia. These processes are disposed in ranks of roughly equally spaced heights, containing (in descending order of height) 2, 4, 3, 4, 5, 4, 5, 4, 5, 4, 5, 4, 3, 4, 3, 3, and 1 stereocilia; the total stereociliary length is therefore ~434 μm. If the apical membrane has the usual specific capacitance of ~10 $mF \cdot m^{-2}$, the round, flat portion of the apical surface contributes an average surface area of ~70 μm^2 and a capacitance of ~0.7 pF. On the basis of light-microscopic observations and of computer modeling of the stacking of stereocilia in hair bundles, the diameter of individual, unfixed stereocilia is ~0.3 μm. With compensation for the tapered bases of the stereocilia and inclusion of the surface area of the single kinocilium, this diameter leads to an estimate of 3.9 pF for the hair bundle's capacitance, and hence of 4.6 pF for the capacitance of the entire apical membrane surface.

slightly when placed in series with the internal conductance along the stereocilium. In series with the >300 pS internal conductance, the maximal transduction conductance of ~50 pS per stereocilium (Holton and Hudspeth, 1986) leads to <15% reduction of the receptor current reaching the cell body.

The corner frequency, f, above which sinusoidal receptor currents suffer significantly greater attenuation, is approximately $f = (2\pi\tau)^{-1}$. Because in this instance $\tau < 110$ μsec, $f > 1.4$ kHz, well above the normal response range of the sacculus (Koyama et al., 1982). These estimates of internal conductance and corner frequency indicate that the stereocilia are efficient cables for transmitting signals from tip to base at all frequencies of physiological relevance to saccular hair cells (Hudspeth, 1982). Moreover, because of the limited frequency response of our voltage-clamp system, we may have overestimated the attenuation by as much as 20-fold; it remains plausible that stereocilia conduct the fastest responses that occur during mechanoelectrical transduction (Corey and Hudspeth, 1979b, 1983b).

Ion channels are clustered on the basolateral surface

In 58 saccular hair cells, we made focal current measurements from 65 basolateral membrane patches 10–1000 μm^2 in area. We found that the current density, the ratio of a patch's current to its area, varied more than 100-fold among patches. This variation, moreover, increased with decreasing patch area. Although most patches contributing less than 5% of the cell's surface area bore no significant ionic current, those patches with measurable currents usually had current densities that exceeded the average current density of the basolateral membrane surface.

Because the apical membrane surface lacks voltage- and ion-activated currents, it was most appropriate to compare a patch's current density with that of the basolateral cellular surface. The basolateral-surface current density was obtained by dividing the whole-cell current by the estimated area of the basolateral membrane surface. This in turn was obtained by subtracting the mean apical surface area of ~400 μm^2 from the surface area estimated from whole-cell capacitance measurements.

Ca^{2+} channels

We measured local Ca^{2+}-channel densities after blocking the Ca^{2+}-activated K^+ current by substituting Cs^+ for K^+ in the intracellular saline solution (Lewis and Hudspeth, 1983a; Art and Fettiplace, 1987; Hudspeth and Lewis, 1988a). The Ca^{2+}-current density varied more than 10-fold among the patches studied (mean, 0.83 of the basolateral-surface density; coefficient of variation, 0.8; 8 patches). Several patches, especially small ones, bore no measurable Ca^{2+} current. At the opposite extreme, the highest current density in a patch was 2.25-fold that of the basolateral surface. In each of the 4 patches with currents large enough to be measured accurately, the patch current had a time course and voltage dependence indistinguishable from that of the whole-cell current (Fig. 9*A*).

Ca^{2+}-activated K^+ channels

Under conditions in which both the Ca^{2+} and the Ca^{2+}-activated K^+ currents were present, depolarizations from −70 to −20 mV evoked whole-cell currents that were transiently inward, but quickly reversed and approached a steady, outward level that

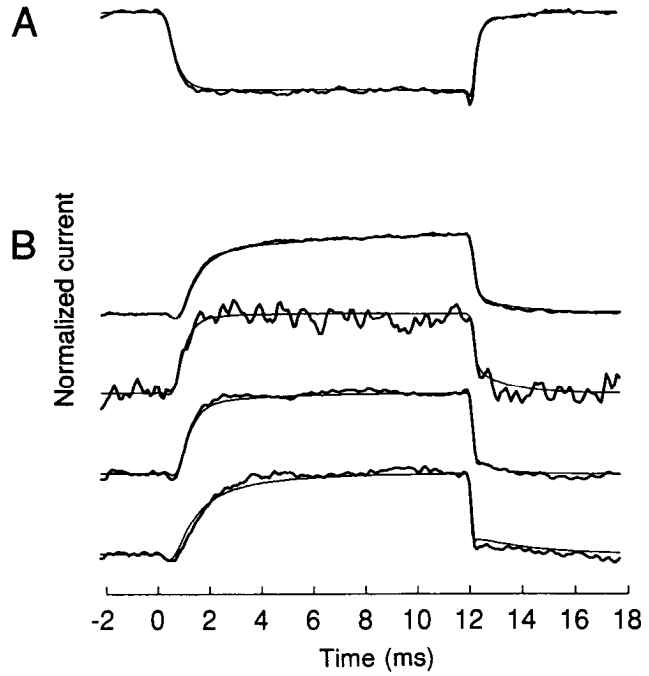

Figure 9. Comparison of whole-cell and focal currents. *A*, Ca^{2+} currents recorded with Cs^+-aspartate internal solution to block the Ca^{2+}-activated K^+ current. The currents during pulses from −70 to −20 mV were normalized to show the similar time courses of the whole-cell (*thin trace*) and focal (*thick trace*) currents. The whole-cell current's greatest amplitude was −934 pA, while the focal current in the patch reached −98 pA; the cell's total membrane area was 1350 μm^2, while the patch's area was 44 μm^2. *B*, Whole-cell and focal currents normalized as in *A*, recorded from 4 different cells with K^+-aspartate internal solution. In this circumstance, both Ca^{2+} and Ca^{2+}-activated K^+ channels were active. Although variability between cells is evident, the focal and whole-cell currents on the same cell show nearly identical time courses. The amplitudes of the steady outward whole-cell and focal currents, the whole-cell and patch areas, and the number of responses averaged were (*top to bottom*) 1397 pA, 607 pA, 2100 μm^2, 769 μm^2, 16 averages; 1541 pA, 94 pA, 1000 μm^2, 35 μm^2, 160 averages; 1446 pA, 125 pA, 1000 μm^2, 26 μm^2, 800 averages; and 2622 pA, 169 pA, 1240 μm^2, 26 μm^2, 160 averages.

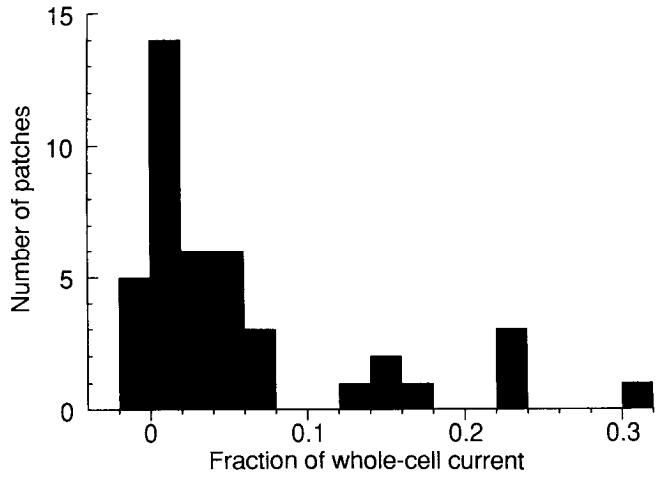

Figure 10. Histogram of distribution of focal outward-current amplitudes, expressed as fraction of whole-cell current to reduce variability due to different physiological conditions of cells. All basolateral patches with areas <200 μm^2 were included. Steady-state outward currents, which were predominantly Ca^{2+}-activated K^+ currents, were recorded at −20 mV in K^+-aspartate internal solution.

was the sum of the inward Ca^{2+} current and an outward K^+ current roughly thrice as large. The focal pipette recorded steady-state current densities that varied between −0.3 and 16.6 times the basolateral-surface current density (mean, 1.04 of the basolateral-surface current density; coefficient of variation, 2.1; 57 patches). After correction for field potentials, 3 small patches had steady-state inward currents of 2–5 pA; these values were not significantly different from 0. The highest current density was recorded from a patch that had an area of 10 μm^2 (<2% of the basolateral surface) and bore 23% of the whole-cell current.

Despite their variable amplitudes, the patch and whole-cell currents had remarkably similar time courses (Fig. 9*B*); the differences among cells were much larger than the differences between the patch and whole-cell currents in the same cell. Furthermore, the ratio of the peak inward to the peak outward current in each patch resembled that in the corresponding whole-cell recording. Both results indicate a strong correlation between the local densities of Ca^{2+} and Ca^{2+}-activated K^+ channels. The failure to find patches with significant steady-state inward currents indicates that all patches containing Ca^{2+} channels also contained K^+ channels. Our assertion that all patches containing K^+ channels also contained Ca^{2+} channels is more tenuous. In some instances, the very short delay between the activation of the Ca^{2+} current and the onset of the Ca^{2+}-activated K^+ current precluded measurement of the peak inward current in both whole-cell and patch-current records (Fig. 9*B*, second trace). For every cell in which the Ca^{2+} current was apparent in the whole-cell recording, however, it was also evident in the patch-current record.

The spatial variation in current density, and the frequent observation of patches that provided little or no current, indicated that a hair cell's Ca^{2+}-activated K^+ channels were not strewn randomly across the basolateral surface and suggested that most of these channels congregated in a few patches. Consistent with this hypothesis, a histogram of the steady-state currents recorded from all 41 small patches showed several discrete peaks that could have arisen if each recording was made from 0–4 clusters of channels, each of which contained ~8% of a cell's channels (Fig. 10).

If the variability in current amplitude seen in Figure 10 were due to the random placement of a small number of channel clusters, then a large variability in current density should have been observed in recordings from patches small enough to contain an average of only 1 cluster. Such patches often should have contained either 0 or 1 cluster, and occasionally 2 or more. Still smaller patches usually should have contained no clusters; when a cluster was present, however, the current density should have been high.

Figure 11 shows that the data exhibited the expected relation between current density and patch area. The median current density was close to the mean basolateral current density in large patches, but declined to near 0 in smaller patches. This indicates that most small patches bore little or no current. Because the decline in median current density occurred in patches smaller than ~5% of the basolateral area, the basolateral surface evidently bears about 20 channel clusters.

To test this hypothesis more rigorously, we fit the data from all patches to a model that assumed that channels were grouped into clusters distributed randomly on the basolateral surface.

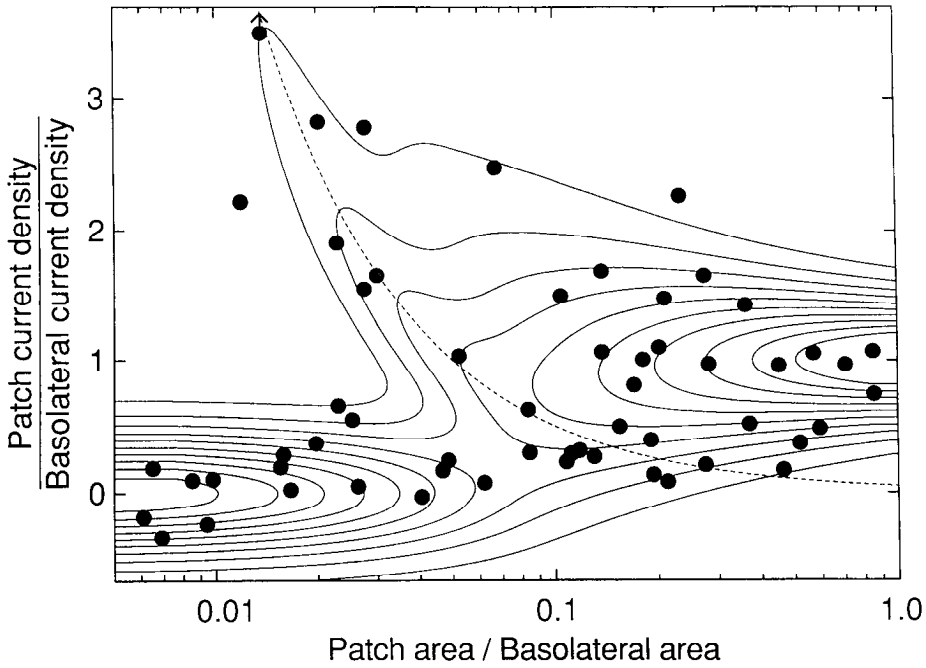

Figure 11. Current densities from all basolateral patches recorded with K^+-aspartate internal solution in whole-cell pipette. As demonstrated in Figure 2, the Ca^{2+}-activated K^+ current dominated the recorded signals. For each *data point,* we measured simultaneously the whole-cell and patch currents, so that we could express patch area and patch current, respectively, as a fraction of the area of, and a fraction of the current in, the entire basolateral surface. This procedure normalized for differences in the sizes and physiological conditions of the cells studied. The basolateral area was estimated by subtracting the average apical capacitance of 4.0 pF from each cell's measured capacitance and assuming a specific capacitance of 10 $mF \cdot m^{-2}$. Each current was measured at −20 mV and converted to a current density by dividing by the membrane area. One point (*arrow*) fell off the scale, with a patch density that was 16.6 times the basolateral current density. The bimodal distribution of current densities observed in patches containing 1.2–6% of the basolateral surface indicates that channels cluster in a few regions of high channel density, rather than being scattered randomly across the cell surface. The solid lines are contours of equal probability density computed from a model in which the channels are concentrated in 20 small clusters distributed randomly on the basolateral surface (see text); contours are shown for probability densities between 0.1 and 1.0 in steps of 0.1. In this model, the scatter in the data recorded from patches containing <1% or >90% of the basolateral surface arises mostly from measurement error ($\sigma_d = 0.32$). In patches containing between 2 and 10% of the basolateral surface, the scatter results primarily from random variation in the number of channel clusters in a patch. The *dashed line* indicates the current densities expected from patches that contain 1 channel cluster apiece.

To minimize the effects of variation in cell size, we expressed focal current density and capacitance measurements as fractions of the current density and capacitance of the entire basolateral surface (Fig. 11). To allow for variability in the number of channel clusters per cell (N_c), we assumed a Poisson distribution. We modeled the measurement error as an additive Gaussian noise with a standard deviation (σ_d) independent of the patch area. A computer program found the best estimates of N_c and σ_d by searching through combinations of these 2 parameters until it encountered the pair that gave the maximum likelihood of generating the data. The estimates were $N_c = 20$ clusters per cell and $\sigma_d = 32\%$ of the average basolateral current density. Any number of clusters between 16 and 27 gave a fit that was not significantly worse than the best fit (likelihood ratio, >0.1). A much worse fit (likelihood ratio, $<10^{-100}$) was obtained on the assumption that individual Ca^{2+}-activated K^+ channels were scattered randomly over the basolateral surface (i.e., $N_c = 700$). Figure 11 shows that the model predicted the observed distribution of current densities for all patch sizes used here. A value of $N_c = 19$ was obtained using current densities and capacitances determined without correction for the field potential (see Materials and Methods). Eliminating the single recording in which the current density was much larger than the rest (arrow in Fig. 11) yielded a best fit of $N_c = 24$.

Because the model was based on assumptions concerning the measurement noise and variability among cells that were necessarily somewhat arbitrary, we tested several different sets of assumptions. All gave similar estimates of the number of clusters per cell. Allowing an additional degree of freedom, a Gaussian distribution in the number of channels per cluster, yielded $N_c = 21$. Allowing no variability in the number of clusters per cell or channels per cluster gave $N_c = 18$. Assuming that the additive current–density noise was the sum of 2 components, one with a standard deviation that was independent of patch area (as before), the other with a standard deviation that was inversely proportional to the patch area (as would arise from noise that had a constant amplitude expressed in units of current), again yielded $N_c = 20$. The close agreement among these different models indicates that the particular assumptions about the type of noise in the data have little effect on the estimated value of N_c. We conclude that there are approximately 20 clusters of Ca^{2+} and Ca^{2+}-activated K^+ channels on the basolateral membrane surface.

Although channel clusters were encountered on every part of the basolateral surface, they were more likely to occur near the basal pole. On average, the current density below the level of the cell nucleus was 2.1 times that above the nucleus.

Electron-microscopic morphometry of synaptic sites

Voltage-gated Ca^{2+} channels are thought to cluster at presynaptic active zones, where they provide the influx of Ca^{2+} that triggers exocytosis (reviewed by Smith and Augustine, 1988). To test

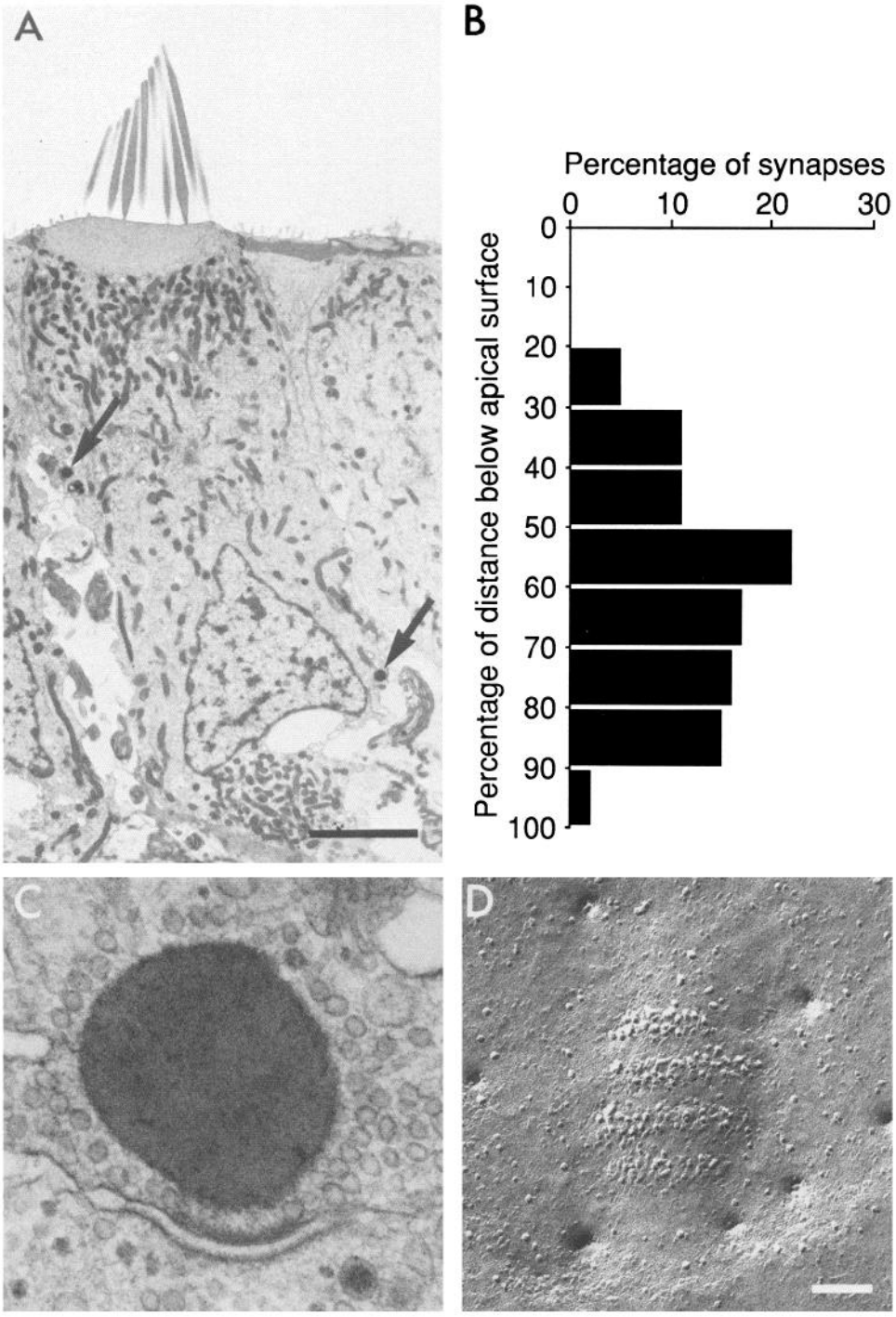

Figure 12. *A*, Transmission electron micrograph of a 200-nm section through a hair cell. The *arrows* point to presynaptic dense bodies. Scale bar, 5 μm. *B*, Histogram showing the spatial distribution of afferent synapses for the 5 cells analyzed in Table 5. The position of each presynaptic dense body is given as the percentage distance between the apical surface (*0%*) and the basal pole (*100%*). *C*, Higher-magnification view of a 100-nm section revealing a halo of round, lucent vesicles surrounding each presynaptic dense body. *D*, Freeze-fracture electron micrograph showing the particle array in the presynaptic membrane at an active zone. This intramembrane specialization contains 125 particles, whose diameters are ~12 nm in this platinum-carbon replica. Scale bar, 100 nm for *C*, *D*.

whether the clusters of ion channels encountered here in electrical recordings coincide with sites where the hair cell releases a chemical transmitter onto afferent axons, we made transmission electron micrographs of serially sectioned hair cells (Fig. 12*A*) to determine the number and spatial distribution of synaptic sites. The task was facilitated by the presence of a large (~400-nm-diameter), osmiophilic presynaptic body (Gleisner et al., 1973; Hama and Saito, 1977) that marked each afferent synapse (Fig. 12*C*). Reconstruction of 5 hair cells from serial sections (Table 5) yielded an average of 18.6 ± 2.3 afferent synapses per cell (mean ± SEM). These sites were distributed along the cell's apical-basal axis (Fig. 12*B*, Table 5) in a fashion similar to that observed for the channel clusters in physiological recordings.

Freeze-fracture measurement of intramembrane particles

In freeze-fracture electron micrographs, a dense cluster of intramembrane particles occurs in the hair cell's membrane at each afferent synapse (Hama, 1980). To investigate whether these particles could correspond to Ca^{2+} channels and Ca^{2+}-activated K^+ channels, we estimated the number of particles per synapse in hair cells from the frog's sacculus. In 4 freeze-fracture

Table 5. Afferent synapses in serially sectioned hair cells

Cell number	Synapses counted	Total sections	Missing sections	Corrected number of synapses	Synapses below nucleus	Area below nucleus	Synaptic density (below nucleus/ above nucleus)
1	20	75	4	21.1	30%	27%	1.2
2	16	93	8	17.4	50%	20%	4.0
3	24	90	8	26.1	17%	19%	0.9
4	13	83	9	14.4	23%	23%	1.0
5	13	115	8	13.9	62%	24%	5.1
	17.2 ± 2.1			18.6 ± 2.3			2.4 ± 0.9

The number of afferent synaptic sites was determined from electron micrographs of 200-nm-thick serial sections of 5 hair cells, printed at a magnification of ~3000×. Synapses were identified by their associated presynaptic bodies. For each synapse, we measured its distance from the apical surface and noted whether it was apical or basal to the nucleus. To compensate for occasional lost sections, we increased the synapse count in proportion to the fraction of sections that were lost to determine the corrected number of synapses. Because each synaptic body was visible in 2–4 sections, we considered a section missing only if it occurred between 2 other lost sections. The surface area of each cell was estimated from its measured length and diameter on the assumption that the basolateral surface was a cylinder with a hemispherical bottom. Each average is expressed as the mean ± SEM.

preparations, we counted the particles in all plaques that could be identified as presynaptic active zones by their characteristic shape (Fig. 12*D*). We found an average of 133 ± 15 particles per synaptic site (mean ± SEM, 13 sites). These and other morphological measurements are summarized in Table 6.

Discussion

We investigated the spatial distribution of the ion channels that mediate 2 important processes in hair cells, electrical tuning and synaptic transmission. We found that these functions are closely linked, both by their colocalization upon the plasmalemmal surface and by their reliance upon a common intracellular messenger. A single population of Ca^{2+} channels appears to provide the influx of Ca^{2+} that triggers exocytosis and opens the Ca^{2+}-activated K^+ channels to generate a cell's electrical resonance. We propose that both types of channels cluster together at afferent synapses, where they can be seen as intramembrane particles in freeze-fracture electron micrographs.

Table 6. Intramembrane particles at presynaptic active zones

Synapse number	Number of particles	Mean particle diameter (nm)	Area of active site (nm²)
1	84	10.7	27,000
2	247	9.2	81,200
3	237	6.9	106,000
4	95	13.1	32,000
5	146	11.0	65,800
6	137	11.0	72,100
7	91	10.9	32,300
8	116	11.2	37,800
9	125	10.8	80,700
10	137	11.8	58,500
11	120	13.5	67,000
12	128	13.5	86,600
13	61	13.4	32,900
	133 ± 15	11.5 ± 0.4	60,000 ± 7100

The number of intramembrane particles was determined from freeze-fracture electron micrographs of presynaptic active zones (Fig. 12*D*) printed at a magnification of ~150,000×. The area of an active zone was defined as the membrane surface area within which particles occurred in linear arrays. Particle counts included both tightly clustered particles and those lying between arrays. Each average is expressed as the mean ± SEM. If the particle arrays were precisely circular, the mean diameter of an active zone would be 276 nm.

Apical-basal polarity

As a constituent of a tight epithelium that isolates the endolymph from the perilymph, each hair cell possesses a tight junction (Jahnke, 1975; Gulley and Reese, 1976); this circumferential membrane specialization couples the cell to adjacent supporting cells and divides its membrane into functionally distinct apical and basolateral domains. Our observation that a hair cell's ion channels are partitioned asymmetrically between its apical and basolateral surfaces is consistent with the general principle that epithelial cells maintain distinct populations of membrane proteins in these 2 regions (Simons and Fuller, 1985). In hair cells, the apical membrane is specialized for mechano-electrical transduction, while the basolateral membrane contains the elements that filter the electrical signal and transmit it to the CNS.

It has been proposed that the tight-junctional ring forms a barrier that maintains epithelial-cell polarity by blocking the lateral diffusion of membrane components (Dragsten et al., 1981). Our finding that the asymmetrical distribution of ion channels persists for at least 2 hr after enzymatic dissociation in low Ca^{2+}, a treatment known to disrupt tight junctions, supports the more recent view that the tight junction is not directly responsible for segregating membrane proteins (for a review, see Cereijido et al., 1989). The nonuniform channel distributions on the basolateral surface additionally indicate that channels are subject to local restraints on diffusion. This observation agrees with results from other cells that have shown most ion channels in fully differentiated cells to be immobilized in the membrane (reviewed by Almers and Stirling, 1984; Poo, 1985).

Specific binding of membrane proteins to cytoskeletal anchors is known to immobilize the anion channels of red blood cells

(Branton et al., 1981) and may maintain locally high densities of ACh receptors (reviewed by Poo, 1985) and Na^+ channels (Caldwell et al., 1986; Weiss et al., 1986; Roberts, 1987) at the neuromuscular junction and of Na^+ channels at the node of Ranvier (reviewed by Waxman and Ritchie, 1985). Although specific binding of ion channels to cytoskeletal proteins that associate with presynaptic active zones is an attractive explanation for the observed channel distributions in hair cells, we cannot rule out other possibilities such as interactions with extracellular components that persist after the cells are dissociated.

Electrical properties of the apical membrane

Our data indicate that a hair cell from the frog's sacculus has few if any voltage- or ion-activated channels on its apical surface; the only ion channels known to lie in the apical membrane are mechanoelectrical transduction channels (Corey and Hudspeth, 1983a). The apical membrane surface of such a hair cell seems to be wholly devoted to mechanoelectrical transduction in much the same way that the plasma membrane of a photoreceptor's outer segment, whose ion channels are almost exclusively light controlled (Baylor and Lamb, 1982), is committed to photoelectrical transduction. Our results contrast with those on mammalian outer hair cells, whose apical surfaces contain uncharacterized, voltage-sensitive channels (Gitter et al., 1986).

Measurements of extracellular field potentials suggest that transduction occurs near the distal ends of stereocilia (Hudspeth, 1982; but see Ohmori, 1988). Because transduction at this site requires that receptor current flows along the narrow stereociliary shafts to the cell body, it could entail significant losses of the high-frequency, oscillatory receptor currents in auditory hair cells. Measurements of the electrical properties of the apical membrane presented in this paper, however, demonstrate that voltage changes imposed at the cell body spread throughout the hair bundle without significant attenuation at the highest frequency that our recording apparatus could measure, ~1.4 kHz. At least up to that frequency, transduction may therefore occur at the tips of hair bundles without untoward attenuation of the resultant signals.

Hair cells have L-type Ca^{2+} channels

Although the hair cells' Ca^{2+} channels are in some respects unlike any other known Ca^{2+} channels, they most closely resemble *L*-type channels in the classification scheme proposed by Nowycky et al. (1985; reviewed by Miller, 1987; Tsien et al., 1988). We base this assignment upon the channels' sensitivity to the dihydropyridine (+)202791 (Fig. 3*A*), lack of inactivation at potentials within the normal physiological range (Lewis and Hudspeth, 1983a; Art and Fettiplace, 1987; Hudspeth and Lewis, 1988a), large single-channel current (see below), greater conductance to Ba^{2+} than Ca^{2+} (Art and Fettiplace, 1987), and propensity for rundown (Fig. 3*D*; Armstrong and Eckert, 1987). The channels are unusual, however, in that they activate at potentials 20–50 mV more negative than do *L*-type channels in most other preparations (Fenwick et al., 1982; Armstrong and Matteson, 1985; Fox et al., 1987a,b; Markwardt and Nilius, 1988; Taylor, 1988; Huang, 1989).

The hair cells' Ca^{2+} current bears a striking resemblance to the presynaptic Ca^{2+} current at the squid's giant synapse (Augustine et al., 1985). The currents activate and deactivate with similar time courses, show little or no inactivation during depolarizations lasting seconds, and share large voltage sensitivities. The squid's channels activate at relatively negative potentials, though not so negative as is characteristic for the hair cell's channels. The only other noninactivating Ca^{2+} channels known to open in a voltage range similar to that of the hair cell's channel, which occur in the inner segments of salamander photoreceptors (Corey et al., 1984; Barnes and Hille, 1989), differ from the hair cell's in that they activate more slowly.

Our estimate of the single-channel Ca^{2+} current (i_{Ca}) is consistent with the channel's classification as an *L*-type channel. Figure 4 shows our estimates of i_{Ca} at several potentials, with and without the dihydropyridine agonist (+)202791. We believe that the values of i_{Ca} obtained with the agonist are more accurate than those obtained without because the drug slows the channel kinetics, bringing a larger fraction of the channel noise within the bandwidth of our recording apparatus. This effect is particularly important at large negative potentials, at which the open times are shortest. Fenwick et al. (1982) used ensemble-variance analysis to estimate $i_{Ca} \approx -90$ fA (at −12 mV, 20–22°C, 5 mM Ca^{2+} as the charge carrier) for the *L*-type channels in bovine chromaffin cells. Our value, which is twice as large ($i_{Ca} \approx -180$ fA at −14 mV, 22–25°C, 4 mM Ca^{2+} as the charge carrier), indicates that the hair cell's channel is a high-conductance, *L*-type channel. The curvature of the open-channel current–voltage relation (Fig. 4) also accords with that reported by Fenwick et al. (1982). At the hair cells' normal operating voltage near −50 mV, the single-channel current is about −0.8 pA.

To participate in electrical resonance at frequencies above 100 Hz, Ca^{2+} channels must be highly voltage dependent and undergo extremely rapid activation and deactivation (Art and Fettiplace, 1987; reviewed by Roberts et al., 1988). The hair cells' Ca^{2+} channels resemble most other *L*-type Ca^{2+} channels (Fox et al., 1987b) in their steep voltage sensitivity (*e*-fold change per 4 mV; Fig. 6*C*), but differ in their rapid activation (half-rise time, 300–800 μsec after a depolarizing step from −70 mV) and deactivation (half-fall time, <300 μsec upon repolarization to −70 mV) at 22–25°C (Figs. 3*A*, 9*A*; Hudspeth and Lewis, 1988a). Rapid Ca^{2+} currents have also been seen in hair cells from the chick's vestibular and the turtle's auditory organs (Ohmori, 1984; Art and Fettiplace, 1987). The Ca^{2+} currents reported in other cell types respond to voltage changes significantly more slowly, at least when measured at room temperature. At mammalian body temperature, *L*-type Ca^{2+} channels from guinea-pig heart (Markwardt and Nilius, 1988) and cat dorsal-root ganglia (Taylor, 1988) operate about as quickly as Ca^{2+} channels in frog hair cells at 22°C.

L-type Ca^{2+} channels mediate transmitter release at afferent synapses

Hair cells excite afferent nerve terminals by the quantal release of a chemical transmitter (Ishii et al., 1971) that is probably stored in the 30–60-nm-diameter, clear-cored vesicles that crowd around the presynaptic body at each active zone (Gleisner et al., 1973; Hama and Saito, 1977). Because we found no evidence for more than 1 class of Ca^{2+} channel, it seems likely that *L*-type channels mediate afferent transmission in hair cells. Although other instances have been found in which noninactivating, dihydropyridine-sensitive channels probably control transmitter release (cultured rat dorsal-root ganglionic neurons, Perney et al., 1986; Holz et al., 1988; rat neurohypophyseal cells, Lemos and Nowycky, 1989), these synapses contain large, dense-cored vesicles and release peptide neurotransmitters. Based upon results from cultured rat superior cervical ganglion cells, PC12 cells, and a variety of synaptosomal preparations, Miller (1987)

suggested that dihydropyridine-insensitive (*N*-type) Ca^{2+} channels mediate the exocytosis of small, clear-cored vesicles at conventional synapses (reviewed by Hirning et al., 1988; Tsien et al., 1988). Hair cells do not fit into this scheme: they evidently use *L*-type channels to mediate the exocytosis of small, clear-cored vesicles.

Properties of Ca^{2+}-activated K^+ channels

Our analysis of whole-cell Ca^{2+}-activated K^+ currents agrees well with the results of previous single-channel recordings (Hudspeth and Lewis, 1988a); our estimate of the single-channel current from ensemble-variance analysis was 7.0 pA (Table 3), near the value of ~8 pA recorded from excised membrane patches in the presence of similar ionic gradients. We therefore conclude that the large-conductance channel studied in excised patches is the predominant source of outward current in intact hair cells. The smaller single-channel current (4.7 pA) that we observed in buffered-Ca^{2+} experiments might have resulted from prolonged exposure to high $[Ca^{2+}]_i$ (Vergara and Latorre, 1983). At fixed Ca^{2+} concentrations, we found a sigmoidal relation between open probability and voltage, with a Boltzmann slope coefficient of 26 mV and a midpoint of +15 mV in 10 μM $[Ca^{2+}]_i$ (Fig. 6*B*). The K^+ channels in excised patches exhibit a similar slope coefficient, 33 mV, but their activation range is shifted in the negative direction and centers on 0 mV (Hudspeth and Lewis, 1988a). The shift in voltage dependence could be due to a Donnan potential that biased the membrane potential by −15 mV relative to the command potential in whole-cell recordings, but not in excised patches (Hudspeth and Lewis, 1988a).

The hair cell's Ca^{2+}-activated K^+ channels are similar to those in cultured rat muscle (Pallotta et al., 1981) and bovine chromaffin cells (Yellen, 1984) in the size of their single-channel currents measured at 22°C with similar ionic gradients and in the saturation (Fig. 6*A*) seen at large positive potentials (Yellen, 1984). The hair cells' channels are slightly less sensitive to Ca^{2+} and moderately less sensitive to voltage than are the large-conductance Ca^{2+}-activated K^+ channels in cultured rat muscle (slope coefficient = 15 mV and 50% activation at −8 mV in 10 μM $[Ca^{2+}]_i$; Barrett et al., 1982).

In view of the need for rapid activation and high voltage sensitivity of the ion channels involved in electrical resonance (Ashmore and Attwell, 1985; Art and Fettiplace, 1987; Roberts et al., 1988), and of the fact that most of the Ca^{2+}-activated K^+ channel's apparent voltage sensitivity is derived from its Ca^{2+} sensitivity (Fig. 6*B*), it was somewhat surprising to find that the hair cell's channels are not particularly sensitive to Ca^{2+}, but require $[Ca^{2+}]_i > 10$ μM to be open more than half of the time at any negative membrane potential. We offer 2 explanations for this finding. First, rapid deactivation in response to hyperpolarization is just as important for resonance as is rapid activation following depolarization (Art and Fettiplace, 1987). An extremely high affinity for Ca^{2+} binding to the channel could only be achieved at the expense of a small *off* rate constant that would slow the channel's deactivation. A minimum dissociation constant (K_d) for Ca^{2+} binding to the channel can be estimated from the channel's known deactivation rate constant of 1–2 msec near the resting potential (Art and Fettiplace, 1987; Hudspeth and Lewis, 1988a). If activation were controlled by a single Ca^{2+}-binding site, with a diffusion-limited association rate constant of $\sim 10^8$ $M^{-1} \cdot s^{-1}$, the highest affinity consistent with a dissociation rate constant of 10^3 sec^{-1} would be $K_d \approx 10$ μM. Although the situation is more complex if the channel has more than one binding site, it is significant that, according to the model of Hudspeth and Lewis (1988a), the Ca^{2+}-activated K^+ channel's 3 binding sites have K_d values (at the cell's normal operating voltage of −55 mV) of 14, 45, and 48 μM, near the theoretical minimum. Consistent with this idea, the highly Ca^{2+}-sensitive channel in acinar cells from mammalian salivary glands (Maruyama et al., 1983, 1986) deactivates with a slow time constant of ~15 msec (at 22°C and at a membrane potential of 0 mV, at which the channel is open roughly half the time in 100 nM $[Ca^{2+}]_i$). Hair cells achieve both a high sensitivity to changes in the Ca^{2+} current and a rapid deactivation rate by clustering channels together, so that small changes in the current produce large changes in the local Ca^{2+} concentration.

A second reason for the Ca^{2+}-activated K^+ channel's having a low affinity for Ca^{2+} is the need for a significant steady-state Ca^{2+} current to permit symmetrical voltage oscillations around the resting potential (Art and Fettiplace, 1987). The Ca^{2+} current's ~2% resting activation (Fig. 6*C*) creates a local $[Ca^{2+}]_i$ near 20 μM; if the binding sites on Ca^{2+}-activated K^+ channels had high Ca^{2+} affinities, this $[Ca^{2+}]_i$ would completely saturate the sites.

Ca^{2+} channels and Ca^{2+}-activated K^+ channels cluster together

Our patch recordings provide direct evidence that both types of channels cluster together in a few patches on the basolateral membrane surface. Given the large variability in the densities of Ca^{2+} channels (coefficient of variation = 0.8) and Ca^{2+}-activated K^+ channels (coefficient of variation = 2.2), the failure to find patches in which the Ca^{2+} current exceeded the K^+ current demonstrates that the 2 channels are not distributed independently. The similar ratios of peak inward to peak outward currents in whole-cell and patch recordings suggest that there is a nearly constant ratio of Ca^{2+} current to K^+ current in all patches on a cell. This inference is supported by the similar time courses of whole-cell and patch currents. To test the possibility that this correlation in *current* density did not indicate a correlation in *channel* density, but instead came about because Ca^{2+} channels could activate only nearby K^+ channels, we sought a population of normally silent K^+ channels that could be opened under conditions of uniformly high $[Ca^{2+}]_i$. None was found.

A statistical analysis (Fig. 11) of how the variability in current density depends upon on patch area suggests that nearly all of the Ca^{2+} and Ca^{2+}-activated K^+ channels occur in ~20 small clusters on the basolateral membrane surface. The insertion or anchoring of the channels is evidently so precise that they are confined to only ~0.1% of the basolateral membrane area. It remains possible that some channels are distributed diffusely on the basolateral surface; however, because the current densities found in the smallest patches scattered around a median value that was <0.2, Figures 10 and 11 indicate that such channels constitute less than 20% of the total population.

The steep relation between Ca^{2+} current and $[Ca^{2+}]_i$ (Fig. 6*D*) and the inability of 66 mM BAPTA to buffer the Ca^{2+} concentration in the vicinity of the Ca^{2+}-activated K^+ channels (Fig. 5*A*) provide further evidence for the colocalization of the 2 types of channels. Marty and Neher (1985) also reported that intracellular Ca^{2+} buffers were inefficient at blocking the Ca^{2+}-activated K^+ current in chromaffin cells. They found that the K^+ current persisted in isotonic EGTA, but was blocked by 5.5 mM

BAPTA. The persistence of the hair cell's K^+ current in a >10-fold higher concentration of BAPTA suggests a closer spatial association between the channels in hair cells than in chromaffin cells. This issue will be discussed in more detail below.

Clusters of ion channels probably correspond to presynaptic active zones

Theoretical treatments of ionic diffusion away from Ca^{2+} channels indicate that there is a steep spatial gradient of intracellular Ca^{2+} concentration in the vicinity of an open Ca^{2+} channel (Chad and Eckert, 1984; Fogelson and Zucker, 1985; Simon and Llinás, 1985). Clustering of Ca^{2+} channels around transmitter-release sites at synapses probably produces a large, rapid change in local intracellular Ca^{2+} concentration ($[Ca^{2+}]_i$) that minimizes the synaptic delay (Fogelson and Zucker, 1985); we believe that the colocalization of Ca^{2+} channels and Ca^{2+}-activated K^+ channels serves a similar function of increasing the activation rate and apparent voltage sensitivity of the hair cells' K^+ channels.

The close correspondence between the average number of active zones and channel clusters per hair cell (~20 of each), as well as the tendency of both to be found towards the basal pole, suggests that the channels are closely associated with synaptic sites. A much stronger argument is possible if one assumes that each active zone produces a measurable Ca^{2+} current. If each cell had 19 afferent synapses and 20 channel clusters that were separate entities distributed independently on the basolateral surface, then a simple statistical calculation shows that the 57 data points shown in Figure 11 should include ~6 recordings from patches that contained 1 or more active zones but no channel clusters that might obscure synaptic Ca^{2+} currents. Because none of the patches had a significant, steady-state inward current, we conclude that if synapses are independent of the channel clusters, then each active zone must have a Ca^{2+} current at −20 mV smaller than −5 pA, the largest inward current measured in these 57 patches. If the average whole-cell Ca^{2+} current of ~1400 pA (Fig. 6*C*) flows through 1800 Ca^{2+} channels, we estimate that $i_{Ca} \approx -0.8$ pA in these experiments. Each active zone would therefore have fewer than 7 Ca^{2+} channels, and less than 7% of the cell's Ca^{2+} channels would be associated with synapses. Although we cannot rule out this possibility, we believe it more likely that a larger fraction of the cell's Ca^{2+} channels are involved in synaptic transmission. The above calculation, in conjunction with the agreement in their number and spatial distribution, leads us to conclude that channel clusters correspond to active zones.

Most hair cells, including those of the frog's sacculus, receive efferent synaptic contacts from neurons in the brain stem or cerebellum. Activation of the efferent innervation or application of the probable efferent neurotransmitter, ACh, generally produces a protracted hyperpolarization in hair cells (Art et al., 1982). By opening ligand-sensitive Ca^{2+} channels or releasing Ca^{2+} from internal stores, the efferent synaptic transmitter might elicit a hyperpolarization by opening Ca^{2+}-activated K^+ channels (Shigemoto and Ohmori, 1990). This hypothesis suggests that there should be membrane patches containing high densities of K^+ channels, but not necessarily any voltage-sensitive Ca^{2+} channels. That we failed to observe such patches could indicate either that efferent synapses are substantially less common than afferent contacts on saccular hair cells, or that the postsynaptic K^+ channels are gated by a second messenger other than Ca^{2+}

Most intramembrane particles at active zones may be ion channels

Several studies have proposed that the intramembrane particles seen in freeze-fracture electron micrographs of transmitter-release sites are Ca^{2+} channels (Heuser et al., 1974; Pumplin et al., 1981; Walrond and Reese, 1985). This hypothesis is based upon the agreement between the number of particles in the presynaptic membrane and rough estimates of the number of Ca^{2+} channels. Our results include accurate counts of both channels and particles, and electrical recordings that show locally high channel densities. They provide the strongest evidence available to date in support of the hypothesis. Dividing the total number of channels per cell (Tables 2, 3) by the number of synapses, we predict that each active zone contains ~90 Ca^{2+} channels and ~40 Ca^{2+}-activated K^+ channels, in good agreement with the observed average of 133 large intramembrane particles per active zone.

The hypothesis that intramembrane particles are ion channels accords with the relation between Ca^{2+} current and local $[Ca^{2+}]_i$

We estimated the intracellular Ca^{2+} concentration near Ca^{2+}-activated K^+ channels by using the channels themselves to assay the local $[Ca^{2+}]_i$ (Fig. 6). Although we report values of $[Ca^{2+}]_i$ that seem extraordinarily high (>1 mM at −40 mV), a simple calculation shows that such concentrations are expected if all of the cell's Ca^{2+} channels are apportioned equally among the cell's ~20 presynaptic sites, where they are confined to a small disk at each active zone. The particles at active zones were generally arrayed in 1 or more short bars (Fig. 12), but we assumed for convenience in calculations that particles were clustered in circular patches 150 nm in radius (Table 6).

The small size of an active zone greatly simplifies the theoretical treatment of local Ca^{2+} diffusion because Ca^{2+} buffering can be ignored over this distance. The argument presented below substantiates this claim for whole-cell recordings made using the K^+-aspartate internal solution, in which the Ca^{2+} concentration was buffered by 1 mM EGTA. Although the Ca^{2+}-buffering capacity of cytoplasm is not known with precision, we believe that similar reasoning applies to Ca^{2+} diffusion in cytoplasm, where the capacity of fast Ca^{2+} buffers is probably well below 1 mM (Simon and Llinás, 1985; Sala and Hernández-Cruz, 1990). If the association rate constant for the binding of Ca^{2+} to EGTA is 9.6×10^6 $M^{-1} \cdot sec^{-1}$, the average time required for a Ca^{2+} ion to encounter and bind to an EGTA molecule in the K^+-aspartate internal solution is ~100 μsec (Neher, 1986). If the diffusion coefficient for Ca^{2+} is 6×10^{-10} $m^2 \cdot sec^{-1}$ (Augustine et al., 1987), this is time enough for the ion to diffuse several hundred nanometers from its point of entry. Within this region, most Ca^{2+} ions are free because they have not yet become bound to buffer molecules. The extent of the unbuffered region is characterized by a space constant (Neher, 1986), which is 250 nm for the K^+-aspartate solution used in our experiments. We can therefore safely ignore buffering within a radius of 150 nm and use the equation for free diffusion from a point source (Smith and Augustine, 1988) to calculate the contribution of an individual Ca^{2+} channel to the local $[Ca^{2+}]_i$ at the center of an active zone:

$$[Ca^{2+}]_i = -i/4\pi FDr, \quad (6)$$

in which i is the single-channel current, F is the Faraday constant, and r is the distance of the channel from the center of the cluster ($r < 150$ nm). The effect of Ca^{2+} entry through many channels in the active zone is simply the sum of the contributions from individual channels: $[Ca^{2+}]_i = (-I/4\pi FD) \times E(1/r)$, in which I is the total Ca^{2+} current through all of the open channels at the active zone and $E(1/r)$ is the value of $1/r$ averaged over all open channels. If channels are distributed randomly within a disk of diameter d, then $E(1/r) = 4/d$, in which r is the distance from the center of the disk. Combining these equations gives the ratio of $[Ca^{2+}]_i$ at the center of the disk to I,

$$\frac{[Ca^{2+}]_i}{I} = \frac{-1}{\pi FDd} = -18\ \mu M/pA. \quad (7)$$

A Ca^{2+}-activated K^+ channel located at the center of the active zone would therefore experience a local $[Ca^{2+}]_i$ of 18 μM per picoampere of Ca^{2+} current. The $[Ca^{2+}]_i$ at the edge of the disk is 65%, and that averaged over the entire disk 84%, of the value at the center. Excluding a 10-nm radius around each Ca^{2+} channel, the average $[Ca^{2+}]_i$ within the disk, and to which Ca^{2+}-activated K^+ channels are exposed, is -13 μM/pA.

These values are in good agreement with the results shown in Figure 6. The slope of the line in Figure 6*D*, which relates local $[Ca^{2+}]_i$ to the whole-cell current, multiplied by the number of active zones per cell, gives a value of 34 μM/pA for the change in $[Ca^{2+}]_i$ caused by the local Ca^{2+} current at each active zone. At membrane potentials between -40 and 0 mV, the average whole-cell Ca^{2+} current exceeded -600 pA, which by Equation 7 corresponds to a local $[Ca^{2+}]_i \approx 1$ mM, in agreement with Figure 6*B*. Although an intracellular Ca^{2+} concentration of 1 mM seems perilously close to the extracellular concentration of 4 mM, it is well below the Nernst equilibrium concentration of 105 mM at -40 mV. The close agreement between the experimental and theoretical Ca^{2+} concentrations supports our hypothesis that all of the cell's Ca^{2+} channels and Ca^{2+}-activated K^+ channels cluster together at ~300-nm-diameter active zones.

Regardless of whether channel clusters correspond to active zones, channels must be clumped together to achieve the high local Ca^{2+} concentrations shown in Figure 6*B*. Equation 6 shows that the Ca^{2+}-binding site on a Ca^{2+}-activated K^+ channel would need to be unreasonably close, within 1.1 nm, to the mouth of a lone Ca^{2+} channel to experience a local $[Ca^{2+}]_i$ of 1 mM (assuming $i_{Ca} = -0.8$ pA). The minimum spacing between channels is probably at least 8 nm (the spacing of hexagonally packed gap-junction connexons; Sikerwar and Unwin, 1988). At this packing density, it is conceivable that 10 Ca^{2+} channels provide the requisite local $[Ca^{2+}]_i$ for a central Ca^{2+}-activated K^+ channel.

In their model of electrical resonance in frog saccular hair cells, Hudspeth and Lewis (1988a) assumed that 98% of the Ca^{2+} entering through Ca^{2+} channels was bound instantaneously to cytoplasmic buffers. This assumption now seems inappropriate because, as we have shown, the Ca^{2+}-activated K^+ channels are located close to Ca^{2+} channels, where cytoplasmic buffers are ineffective. This finding does not change the overall results of their simulations, however, for an increase in the fraction of Ca^{2+} not bound by buffers (U) can be completely compensated by a corresponding increase in the fraction of the cellular volume in which Ca^{2+} accumulates (ξ).

Conclusions

While the finding that Ca^{2+} channels cluster with Ca^{2+}-activated K^+ channels was expected from the theoretical considerations presented above, their colocalization with synaptic sites was not. We speculate that clumping both channels together at synapses is a means to make the most efficient use of the cells' Ca^{2+} channels. It may also provide the mechanism by which the ratio of Ca^{2+} channels to Ca^{2+}-activated K^+ channels is regulated. For example, each active zone may contain a fixed number of anchorages that hold the correct number of each type of channel in a tight cluster. It will be interesting to investigate whether hair cells of tonotopically organized epithelia, in which the number of Ca^{2+}-activated K^+ channels in a cell is closely correlated with its resonant frequency (Art and Fettiplace, 1987), accomplish this by varying either the number of synapses per cell (Miller and Beck, 1988; Sneary, 1988) or channels per synapse, and whether the differences in kinetics of these cells' Ca^{2+}-activated K^+ channels are related to either the ratio of the 2 channel types or the size of active zones. Experiments of this type will be important for comprehension of the molecular basis of frequency tuning in auditory systems that make use of electrically resonant hair cells.

Because the close association between Ca^{2+}-activated K^+ channels and synapses is probably a specialization related to hair cells' requirements for high-frequency resonance, and not a feature of synapses in general, it will be interesting to look for unusual features of hair cells' channels and synapses that relate to channel localization. For example, the Ca^{2+}-activated K^+ channels might have a cytoplasmic domain that binds specifically to cytoskeletal elements at active zones. Alternatively, hair cells may incorporate into their active zones cytoskeletal proteins that bind to a domain found in all Ca^{2+}-activated K^+ channels. Although data on these subjects will probably have to await the molecular characterization of Ca^{2+}-activated K^+ channels, recent advances with other types of ion channels give hope that we do not have long to wait. Determining the molecular mechanisms by which hair cells distribute their Ca^{2+} channels and Ca^{2+}-activated K^+ channels would be an important piece in the much larger puzzle of how neurons and other excitable cells regulate the spatial distributions of the many types of ion channels on their surfaces.

References

Almers W, Stirling C (1984) Distribution of transport proteins over animal cell membranes. J Membr Biol 77:169–186.

Armstrong D, Eckert R (1987) Voltage-activated calcium channels that must be phosphorylated to respond to membrane depolarization. Proc Natl Acad Sci USA 84:2518–2522.

Armstrong CM, Matteson DR (1985) Two distinct populations of calcium channels in a clonal line of pituitary cells. Science 227:65–67.

Art JJ, Fettiplace R (1987) Variation of membrane properties in hair cells isolated from the turtle cochlea. J Physiol (Lond) 385:207–242.

Art JJ, Crawford AC, Fettiplace R, Fuchs PA (1982) Efferent regulation of hair cells in the turtle cochlea. Proc R Soc Lond [Ser B] 216:377–384.

Ashmore JF (1983) Frequency tuning in a frog vestibular organ. Nature 304:536–538.

Ashmore JF, Attwell D (1985) Models for electrical tuning in hair cells. Proc R Soc Lond [Ser B] 226:325–344.

Augustine GJ, Charlton MP, Smith SJ (1985) Calcium entry into voltage-clamped presynaptic terminals of squid. J Physiol (Lond) 367:143–162.

Augustine GJ, Charlton MP, Smith SJ (1987) Calcium action in synaptic transmitter release. Annu Rev Neurosci 10:633–693.
Barnes S, Hille B (1989) Ionic channels of the inner segment of tiger salamander cone photoreceptors. J Gen Physiol 94:719–743.
Barrett JN, Magleby KL, Pallotta BS (1982) Properties of single calcium-activated potassium channels in cultured rat muscle. J Physiol (Lond) 331:211–230.
Baylor DA, Lamb TD (1982) Local effects of bleaching in retinal rods of the toad. J Physiol (Lond) 328:49–71.
Bledsoe SC Jr (1986) Pharmacology and neurotransmission of sensory transduction in the inner ear. Semin Hearing 7:117–137.
Branton D, Cohen CM, Tyler J (1981) Interaction of cytoskeletal proteins on the human erythrocyte membrane. Cell 24:24–32.
Caldwell JH, Campbell DT, Beam KG (1986) Na channel distribution in vertebrate skeletal muscle. J Gen Physiol 87:907–932.
Cereijido M, Contreras RG, Gonzales-Mariscal L (1989) Development and alteration of polarity. Annu Rev Physiol 51:785–795.
Chad JE, Eckert R (1984) Calcium domains associated with individual channels can account for anomalous voltage relations of Ca-dependent responses. Biophys J 45:993–999.
Cochran SL, Kasik P, Precht W (1987) Pharmacological aspects of excitatory synaptic transmission to second-order vestibular neurons in the frog. Synapse 1:102–123.
Conti F, Hille B, Nonner W (1984) Non-stationary fluctuations of the potassium conductance at the node of Ranvier of the frog. J Physiol (Lond) 353:199–230.
Corey DP, Hudspeth AJ (1979a) Ionic basis of the receptor potential in a vertebrate hair cell. Nature 281:675–677.
Corey DP, Hudspeth AJ (1979b) Response latency of vertebrate hair cells. Biophys J 26:499–506.
Corey DP, Hudspeth AJ (1983a) Analysis of microphonic potential of the bullfrog's sacculus. J Neurosci 3:942–961.
Corey DP, Hudspeth AJ (1983b) Kinetics of the receptor current in bullfrog saccular hair cells. J Neurosci 3:962–976.
Corey DP, Dubinsky JM, Schwartz EA (1984) The calcium current in inner segments of rods from the salamander (*Ambystoma tigrinum*) retina. J Physiol (Lond) 354:557–575.
Crawford AC, Fettiplace R (1980) The frequency selectivity of auditory nerve fibres and hair cells in the cochlea of the turtle. J Physiol (Lond) 306:79–125.
Crawford AC, Fettiplace R (1981) An electrical tuning mechanism in turtle cochlear hair cells. J Physiol (Lond) 312:377–412.
Dragsten PR, Blumenthal R, Handler JS (1981) Membrane asymmetry in epithelia: is the tight junction a barrier to diffusion in the plasma membrane? Nature 294:718–722.
Fenwick EM, Marty A, Neher E (1982) Sodium and calcium channels in bovine chromaffin cells. J Physiol (Lond) 331:599–635.
Fettiplace R (1987) Electrical tuning of hair cells in the inner ear. Trends Neurosci 10:421–425.
Fogelson AL, Zucker RS (1985) Presynaptic calcium diffusion from various arrays of single channels. Implications for transmitter release and synaptic facilitation. Biophys J 48:1003–1017.
Fox AP, Nowycky MC, Tsien RW (1987a) Kinetic and pharmacological properties distinguishing three types of calcium currents in chick sensory neurones. J Physiol (Lond) 394:149–172.
Fox AP, Nowycky MC, Tsien RW (1987b) Single-channel recordings of three types of calcium channels in chick sensory neurones. J Physiol (Lond) 394:173–200.
Fuchs AP, Nagai T, Evans MG (1988) Electrical tuning in hair cells isolated from the chick cochlea. J Neurosci 8:2460–2467.
Gitter AH, Zenner H-P, Frömter E (1986) Membrane potential and ion channels in isolated outer hair cells of guinea pig cochlea. ORL J Otorhinolaryngol Relat Spec 48:68–75.
Gleisner L, Flock Å, Wersäll J (1973) The ultrastructure of the afferent synapse on hair cells in the frog labyrinth. Acta Otolaryngol 76:199–207.
Gulley RL, Reese TS (1976) Intercellular junctions in the reticular lamina of the organ of Corti. J Neurocytol 5:479–507.
Hama K (1980) Fine structure of the afferent synapse and gap junctions on the sensory hair cell in the saccular macula of goldfish: a freeze-fracture study. J Neurocytol 9:845–860.
Hama K, Saito K (1977) Fine structure of the afferent synapse of the hair cells in the saccular macula of the goldfish, with special reference to the anastomosing tubules. J Neurocytol 6:361–373.
Heuser JE, Reese TS, Landis DMD (1974) Functional changes in frog neuromuscular junctions studied with freeze-fracture. J Neurocytol 3:109–131.
Hille B (1984) Ionic channels of excitable membranes, pp 184–186. Sunderland, MA: Sinauer.
Hirning LD, Fox AP, McCleskey EW, Olivera BM, Thayer SA, Miller RJ, Tsien RW (1988) Dominant role of *N*-type Ca^{2+} channels in evoked release of norepinephrine from sympathetic neurons. Science 239:57–61.
Holton T, Hudspeth AJ (1986) The transduction channel of hair cells from the bull-frog characterized by noise analysis. J Physiol (Lond) 375:195–227.
Holz GG IV, Dunlap K, Kream RM (1988) Characterization of the electrically evoked release of substance P from dorsal root ganglion neurons: methods and dihydropyridine sensitivity. J Neurosci 8:463–471.
Howard J, Roberts WM, Hudspeth AJ (1988) Mechanoelectrical transduction by hair cells. Annu Rev Biophys Biophys Chem 17:99–124.
Huang L-YM (1989) Calcium channels in isolated rat dorsal horn neurones, including labelled spinothalamic and trigeminothalamic cells. J Physiol (Lond) 411:161–177.
Hudspeth AJ (1982) Extracellular current flow and the site of transduction by vertebrate hair cells. J Neurosci 2:1–10.
Hudspeth AJ (1986) The ionic channels of a vertebrate hair cell. Hearing Res 22:21–27.
Hudspeth AJ (1989) How the ear's works work. Nature 341:397–404.
Hudspeth AJ, Lewis RS (1988a) Kinetic analysis of voltage- and ion-dependent conductances in saccular hair cells of the bull-frog, *Rana catesbeiana*. J Physiol (Lond) 400:237–274.
Hudspeth AJ, Lewis RS (1988b) A model for electrical resonance and frequency tuning in saccular hair cells of the bull-frog, *Rana catesbeiana*. J Physiol (Lond) 400:275–297.
Ishii Y, Matsuura S, Furukawa T (1971) Quantal nature of transmission at the synapse between hair cells and eighth nerve fibers. Jpn J Physiol 21:79–89.
Jahnke K (1975) The fine structure of freeze-fractured intercellular junctions in the guinea pig inner ear. Acta Otolaryngol [Suppl] 336: 5–40.
Kinnamon SC, Dionne VE, Beam KG (1988) Apical localization of K^+ channels in taste cells provides the basis for sour taste transduction. Proc Natl Acad Sci USA 85:7023–7027.
Koyama H, Lewis ER, Leverenz EL, Baird RA (1982) Acute seismic sensitivity in the bullfrog ear. Brain Res 250:168–172.
Kroese ABA, Das A, Hudspeth AJ (1989) Blockage of the transduction channels of hair cells in the bullfrog's sacculus by aminoglycoside antibiotics. Hearing Res 37:203–218.
Lemos JR, Nowycky MC (1989) Two types of calcium channels coexist in peptide-releasing vertebrate nerve terminals. Neuron 2:1419–1426.
Lewis RS, Hudspeth AJ (1983a) Voltage- and ion-dependent conductances in solitary vertebrate hair cells. Nature 304:538–541.
Lewis RS, Hudspeth AJ (1983b) Frequency tuning and ionic conductances in hair cells of the bullfrog's sacculus. In: Hearing—physiological bases and psychophysics (Klinke R, Hartmann R, eds), pp 17–22. Berlin: Springer.
Markwardt F, Nilius B (1988) Modulation of calcium channel currents in guinea-pig single ventricular heart cells by the dihydropyridine Bay K 8644. J Physiol (Lond) 399:559–575.
Martell AE, Smith RM (1974) Critical stability constants, Vol 1, p 269. New York: Plenum.
Marty A, Neher E (1983) Tight-seal whole-cell recording. In: Single-channel recording (Sakmann B, Neher E, eds), pp 107–122. New York: Plenum.
Marty A, Neher E (1985) Potassium channels in cultured bovine adrenal chromaffin cells. J Physiol (Lond) 367:117–141.
Maruyama Y, Gallacher DV, Petersen OH (1983) Voltage and Ca^{2+}-activated K^+ channel in baso-lateral acinar cell membranes of mammalian salivary glands. Nature 302:827–829.
Maruyama Y, Nishiyama A, Izumi T, Hoshimiya N, Petersen OH (1986) Ensemble noise and current relaxation analysis of K^+ current in single isolated salivary acinar cells from rat. Pflügers Arch 406:69–72.
Miller RJ (1987) Multiple calcium channels and neuronal function. Science 235:46–52.
Miller MR, Beck J (1988) Auditory hair cell innervational patterns in lizards. J Comp Neurol 271:604–628.
Neher E (1986) Concentration profiles of intracellular calcium in the presence of a diffusible chelator. Exp Brain Res Ser 14:80–96.

Nowycky MC, Fox AP, Tsien RW (1985) Three types of neuronal calcium channel with different calcium agonist sensitivity. Nature 316:440–443.

Ohmori H (1984) Studies of ionic currents in the isolated vestibular hair cell of the chick. J Physiol (Lond) 350:561–581.

Ohmori H (1988) Mechanical stimulation and fura-2 fluorescence in the hair bundle of dissociated hair cells of the chick. J Physiol (Lond) 399:115–137.

Pallotta BS, Magleby KL, Barrett JN (1981) Single channel recordings of Ca^{2+}-activated K^+ currents in rat muscle cell culture. Nature 293: 471–474.

Perney TM, Hirning LD, Leeman SE, Miller RJ (1986) Multiple calcium channels mediate neurotransmitter release from peripheral neurons. Proc Natl Acad Sci USA 83:6656–6659.

Poo MM (1985) Mobility and localization of proteins in excitable membranes. Annu Rev Neurosci 8:369–406.

Pumplin DW, Reese TS, Llinás R (1981) Are the presynaptic membrane particles the calcium channels? Proc Natl Acad Sci USA 78: 7210–7213.

Roberts WM (1979) Optimal recognition of neuronal waveforms. Biol Cybern 35:73–80.

Roberts, WM (1987) Sodium channels near end-plates and nuclei of snake skeletal muscle. J Physiol (Lond) 388:213–232.

Roberts WM, Hudspeth AJ (1987a) Spatial distribution of ion channels in hair cells of the bullfrog's sacculus. Biophys J 51:203a.

Roberts WM, Hudspeth AJ (1987b) Co-localization of Ca channels with Ca-activated K channels in hair cells of the bullfrog's sacculus. Soc Neurosci Abstr 13:177.

Roberts WM, Howard J, Hudspeth AJ (1988) Hair cells: transduction, tuning, and transmission in the inner ear. Annu Rev Cell Biol 4:63–92.

Roberts WM, Jacobs RA, Hudspeth AJ (1990) Presynaptic calcium concentration exceeds one millimolar in frog saccular hair cells. Biophys J 57:303a.

Sakmann B, Neher E (1983) Geometric parameters of pipettes and membrane patches. In: Single-channel recording (Sakmann B, Neher E, eds), pp 37–51. New York: Plenum.

Sala F, Hernández-Cruz A (1990) Calcium diffusion modeling in a spherical neuron. Relevance of buffering properties. Biophys J 57: 313–324.

Sewell WF, Mroz EA (1987) Neuroactive substances in inner ear extracts. J Neurosci 7:2465–2475.

Shigemoto T, Ohmori H (1990) Muscarinic agonists and ATP increase the intracellular Ca^{2+} concentration in chick cochlear hair cells. J Physiol (Lond) 420:127–148.

Sigworth FJ (1980) The variance of sodium current fluctuations at the node of Ranvier. J Physiol (Lond) 307:97–129.

Sikerwar SS, Unwin N (1988) Three-dimensional structure of gap junctions in fragmented plasma membranes from rat liver. Biophys J 54:113–119.

Simon SM, Llinás RR (1985) Compartmentalization of the submembrane calcium activity during calcium influx and its significance in transmitter release. Biophys J 48:485–498.

Simons K, Fuller SD (1985) Cell surface polarity in epithelia. Annu Rev Cell Biol 1:243–285.

Smith SJ, Augustine GJ (1988) Calcium ions, active zones and synaptic transmitter release. Trends Neurosci 11:458–464.

Sneary MG (1988) Auditory receptor of the red-eared turtle: II. Afferent and efferent synapses and innervation patterns. J Comp Neurol 276:588–606.

Stühmer W, Roberts WM, Almers W (1983) The loose patch clamp. In: Single-channel recording (Sakmann B, Neher E, eds), pp 123–132. New York: Plenum.

Sugihara I, Furukawa T (1989) Morphological and functional aspects of two different types of hair cells in the goldfish sacculus. J Neurophysiol 62:1330–1343.

Tank DW, Wu E-S Webb WW (1982) Enhanced molecular diffusibility in muscle membrane blebs: release of lateral constraints. J Cell Biol 92:207–212.

Taylor WR (1988) Two-suction-electrode voltage-clamp analysis of the sustained calcium current in cat sensory neurones. J Physiol (Lond) 407:405–432.

Tsien RW, Lipscombe D, Madison DV, Bley KR, Fox AP (1988) Multiple types of neuronal calcium channels and their selective modulation. Trends Neurosci 11:431–438.

Tsien RY (1980) New calcium indicators and buffers with high selectivity against magnesium and protons: design, synthesis, and properties of prototype structures. Biochemistry 19:2396–2404.

Vergara C, Latorre R (1983) Kinetics of Ca^{2+}-activated K^+ channels from rabbit muscle incorporated into planar bilayers. J Gen Physiol 82:543–568.

Walrond JP, Reese TS (1985) Structure of axon terminals and active zones at synapses on lizard twitch and tonic muscle fibers. J Neurosci 5:1118–1131.

Waxman SG, Ritchie JM (1985) Organization of ion channels in the myelinated nerve fiber. Science 228:1502–1507.

Weiss RE, Roberts WM, Stühmer W, Almers W (1986) Mobility of voltage-dependent ion channels and lectin receptors in the sarcolemma of frog skeletal muscle. J Gen Physiol 87:955–983.

Yellen G (1984) Ionic permeation and blockade in Ca^{2+}-activated K^+ channels of bovine chromaffin cells. J Gen Physiol 84:157–186.